

University of Alberta

**A Study of the Colloidal Stability of Mixed Abrasive Slurries of Silica
and Ceria Nanoparticles for Chemical Mechanical Polishing**

by

Fangjian Lin

A thesis submitted to the Faculty of Graduate Studies and Research
in partial fulfillment of the requirements for the degree of

Master of Science

in

Materials Engineering

Department of Chemical and Materials Engineering

©Fangjian Lin
Fall 2011
Edmonton, Alberta

Permission is hereby granted to the University of Alberta Libraries to reproduce single copies of this thesis and to lend or sell such copies for private, scholarly or scientific research purposes only. Where the thesis is converted to, or otherwise made available in digital form, the University of Alberta will advise potential users of the thesis of these terms.

The author reserves all other publication and other rights in association with the copyright in the thesis and, except as herein before provided, neither the thesis nor any substantial portion thereof may be printed or otherwise reproduced in any material form whatsoever without the author's prior written permission.

DEDICATION

This thesis is dedicated to my father Shengyu Lin and my mother Mulian Li, without whom this would not have been possible at all, for their everlasting love, teaching and encouragement as well as financial and moral support through every single step of my life. A special dedication is given to my sister Liping Lin for her support and companionship and the example she set for me. I also would like to dedicate this work to my grandparents, of whom I have been so proud, for the enormous efforts they devoted to raising the whole family during the difficult periods of late 1950s to early 1980s.

ABSTRACT

Slurry stability is an important factor in Chemical Mechanical Polishing (CMP) efficiency. However, few studies have been done in this respect. In settling tests at pH 4, adding various amounts of ceria to colloidal silica slurries was shown to change the stability of the resulted mixed abrasive slurries (5 wt% of silica). Within a range of ceria-to-silica weight ratios, known as the transition range, the mixed abrasive slurries were observed to be unstable. A mathematical estimation based on zero net surface charge was proposed. The modification of particle surface charges through the attachment of positively charged ceria particles to negatively charged silica particles made the mixed slurries unstable. TEM images confirmed such attachments at pH 4. Compared to the slurries containing a single kind of particle, such mixed abrasive slurries were more effective in the CMP of PECVD oxide under the same conditions

ACKNOWLEDGEMENT

I would like to thank my supervisors, Dr. Kenneth Cadien and Dr. Zhenghe Xu, for their professional guidance in my thesis. Dr. Cadien has been extremely supportive through my two-year study within his group, both academically and personally. Dr. Cadien and Dr. Xu have given me very insightful comments, suggestions and help, which contributed immeasurably to the being of this thesis, and were greatly appreciated.

I also would like to thank many group members of Dr. Xu and Dr. Cadien, especially Lucy Nolan and Chendi Wu, for the meaningful discussions and help. Special and sincere thanks are given to my colleague Mr. Amir Afshar for his valuable help with the operations of the TEM system. I thank Mr. James Skwarok of Dr. Xu's group for his technical and administrative support.

In addition, financial support for this study from the Natural Sciences and Engineering Research Council of Canada (NSERC) is greatly appreciated. I am also very grateful to Nyacol Nano Technologies and AkzoNobel for supplying the slurries used in this work. Finally I would like to thank my parents and my sister for their love and support throughout my pursuit of the degree of Master of Science at the University of Alberta.

TABLE OF CONTENTS

CHAPTER 1 INTRODUCTION.....	1
1.1 PLANARIZATION TECHNIQUES.....	1
1.2 CHEMICAL MECHANICAL POLISHING.....	4
1.2.1 General Review of CMP.....	4
1.2.2 Advantages and Disadvantages of CMP.....	5
1.2.3 Future and Challenges of CMP.....	6
1.3 CMP OF DIELECTRIC MATERIALS.....	8
1.3.1 Isolation Techniques: LOCOS & STI.....	8
1.3.2 Interlayer Dielectric CMP.....	9
1.3.3 Shallow Trench Isolation CMP.....	10
1.3.4 Mixed Abrasive Slurries for STI CMP.....	11
1.4 ZETA POTENTIAL (ζ -POTENTIAL).....	13
1.5 SUMMARY OF INTRODUCTION.....	14
CHAPTER 2 EXPERIMENTAL PROCEDURES.....	15
2.1 MATERIALS & SAMPLES PREPARATION.....	15
2.1.1 Materials.....	15
2.1.2 Samples Preparation.....	15
2.2 PARTICLE SIZE DISTRIBUTION.....	16
2.3 ZETA POTENTIAL MEASUREMENTS.....	16
2.3.1 Malvern Nano ZS Zetasizer.....	17
2.3.2 Zetaphoremeter III (SEPHY/CAD).....	18
2.4 SETTLING TESTS OF MIXED ABRASIVE SLURRIES.....	19
2.5 TRANSMISSION ELECTRON MICROSCOPY.....	19
2.6 PLASMA ENHANCED CVD (PECVD).....	20
2.7 CMP WITH MIXED ABRASIVE SLURRIES.....	20
CHAPTER 3 RESULTS & DISCUSSIONS.....	22
3.1 PARTICLE SIZES.....	22
3.2 ZETA POTENTIALS & SETTLING TESTS RESULTS.....	23

3.2.1	Zeta Potentials of Individual Particles.....	23
3.2.2	Initial Settling Tests of Mixed Abrasive Slurries.....	25
3.2.3	Model Proposal Based on Zero Net Surface Charge.....	26
3.2.4	Verification of Model.....	28
3.2.5	Zeta Potential Distributions.....	31
3.2.6	Stability of Mixed Abrasive Slurries.....	37
3.3	TEM RESULTS.....	40
3.3.1	TEM of Ceria-Coated Silica Made at pH 4.....	40
3.3.2	TEM of Ceria/Silica Made at pH 10.....	41
3.4	CMP EFFICIENCY OF MIXED ABRASIVE SLURRIES.....	44
3.4.1	Effect of Ceria Addition to Silica on CMP of Oxide.....	44
3.4.2	Effect of Ceria Addition to Silica on CMP of Nitride.....	47
3.4.3	Comparison of CMP Efficiency at Different pHs.....	49
3.4.4	Schematic Model of Oxide CMP at pH 4.....	50
CHAPTER 4 CONCLUSIONS & RECOMMEDATION.S.....		53
4.1	CONCLUSIONS.....	53
4.2	FUTURE WORK RECOMMENDATIONS.....	54
REFERENCES.....		55

LIST OF TABLES

Table 1 Summary of process parameters used in Chemical Mechanical Polishing of silicon dioxide and silicon nitride.....	21
Table 2 Summary of average particle sizes of silica and ceria (5.44 nm is the primary size of ceria) used in this study.....	23

LIST OF FIGURES

Figure 1 Schematic diagram of surface topography buildup without planarization—Layer 1: Deposited then etched; Layer 2: Deposited without following planarization; Layer 3: Deposited and patterned; Layer 4: Deposited.....	1
Figure 2 (a) schematic diagram of Chemical Mechanical Polishing process, (b) contact mechanism between slurry abrasives, polishing pad and wafer surface during Chemical Mechanical Polishing.....	4
Figure 3 Input parameters that affect the results of Chemical Mechanical Polishing and output results of Chemical Mechanical Polishing.....	5
Figure 4 A typical process flow of Local Oxidation of Silicon for device isolation in Integrated Circuits.....	8
Figure 5 An illustration of electrical double layer and zeta potential.....	13
Figure 6 A photo of Zetaphoremeter III for zeta potential distribution characterization (left: analyzing software; right: measuring system).....	18
Figure 7 Screen Captures of Particle Size Distributions by intensity (%) at pH 4—a) Ceria Slurry; b) Silica EB6080; c) Silica EB6040; d) Silica BZ.....	22
Figure 8 Zeta potentials of silica (EB6080), nitride and ceria as a function of pH, measured by Malvern Nano ZS Zetasizer.....	24
Figure 9 Photos of settling of mixed abrasive slurries at pH 4 with ceria-to-silica weight ratio of (left to right): 0.2, 0.5, 1, 1.6 and 3.2 (silica EB6080 5wt%).....	25
Figure 10 Effect of ceria addition to the zeta potential of silica (0.5wt %) particles, and the effect of silica particle sizes on the transition range at pH 4.....	29

Figure 11 Experimental and Model Iso-Electric Points (IEP) of weight ratio at pH=4 (silica weight 0.5 wt%) as a function of silica particle size).....	30
Figure 12 Zeta potential distributions of individual particles (upmost: Silica; bottom-most: Ceria), mixed abrasive slurries at various ceria to silica weight ratios (0.05, 0.1 and 0.4) at pH 4, measured by Zetaphorometer III.....	33
Figure 13 Average zeta potentials of ceria with silica (EB6080—132.2 nm) at pH 4 (square), at pH 10 (circle), and ceria with silica (BZ—32.5 nm) at pH 4 (triangle), using Zetaphoremeter III.....	35
Figure 14 Shift of zeta potential distributions due to change of silica particle size	36
Figure 15 Settling of mixed abrasive slurries at pH 4 (Silica EB6080) with ceria-to-silica weight ratio from left to right: 0.02, 0.05, 0.1, 0.2 and 0.3 (silica 5wt%).....	38
Figure 16 Settling of mixed abrasive slurries at pH 4 (Silica BZ) with ceria-to-silica weight ratio from left to right: 0.02, 0.05, 0.1, 0.2 and 0.3 (silica 5wt%).....	39
Figure 17 TEM images: (a) silica EB6080 particles—100k ×; (b) ceria particles—250k×; (c) mixture of ceria with silica particles at weight ratio of 0.1—250k×; (d) mixture at weight ratio of 0.1—500k. (samples were made at pH4).....	40
Figure 18 TEM image of ceria with silica particles (dried from solution at pH 10).....	42
Figure 19 Oxide Removal Rates as a function of down pressure using silica (5wt%) slurries and mixed slurries containing 5wt% of silica EB6080 and 1wt% of ceria at pH 4.....	44

Figure 20 A comparison of oxide polishing rates using silica slurry (5wt%), ceria slurries (0.1wt%, 0.5wt% and 1.5wt% from left to right) and mixed slurries of silica and ceria at pH 4.....	46
Figure 21 Nitride Removal Rates as a function of down pressure using silica (5 wt%) slurries and mixed slurries containing 5 wt% of silica EB6080 and 1 wt% of ceria at pH 4.....	47
Figure 22 Nitride Removal Rate with Slurries of higher weight ratios than 0.2 at pH 4, as a function of down pressure.....	49
Figure 23 Comparison of materials removal rates at pH 4 and pH 10 using mixed abrasive slurries with ceria-to-silica weight ratio of 0.1.....	50
Figure 24 Schematic diagram of oxide polishing model at pH 4 for various weight ratios: (a) very low weight ratio i.e. 0.02, particles negatively charged; (b) weight ratios of transition range, particles slightly charged or near-zero charge; (c) higher weight ratios, i.e. 0.2 and above, particles positively charged	52

LIST OF SYMBOLS & ACRONYMS

DoF	Lithographic Depth of Focus (nm)
λ	wavelength of light (nm)
NA	Numerical Aperture
R	the hydrodynamic radius (nm)
k	the Boltzmann constant (J/K)
T	temperature (K)
η	viscosity of the dispersion media (Pa•s)
D	diffusion coefficient (m^2/s)
v	particle velocity (m/s)
E	the electric field applied (V/m)
μ_e	electrophoretic mobility of particles ($m^2V^{-1} s^{-1}$)
ϵ_r	dielectric constant of dispersant.
ϵ_0	permittivity of free space ($C^2 N^{-1} m^{-2}$)
ζ	zeta potential of the particle (mV)
ρ	density of particles ($g\cdot cm^{-3}$)
BPSG	Borophosphosilicate Glass
CMP	Chemical Mechanical Polishing
CVD	Chemical Vapor Deposition
DLS	Dynamic Light Scattering
ILD	Interlayer Dielectric
LOCOS	Local Oxidation of Silicon
PE-CVD	Plasma Enhanced CVD
STI	Shallow Trench Isolation
SOG	Spin On Glass
TEOS	Tetraethyl Orthosilicate
ULSI	Ultra Large Scale Integration
WIDNU	Within Die Non-Uniformity
WIWNU	Within Wafer Non-Uniformity

CHAPTER 1 INTRODUCTION

1.1 PLANARIZATION TECHNIQUES

The outcome of semiconductor technology has been seen in many aspects of our daily life: computers with faster and faster speed, smart mobile phones, the safer cars we drive, the music players we listen to to list a few. The convenience of this technology is based on the nanofabrication of millions of transistors on silicon substrates, which are the building blocks of integrated circuits within silicon chips.

The fabrication process starts from a planar surface of silicon wafer after a cleaning step. As the bare silicon wafer goes through deposition, etching, and re-deposition of layers of various materials, the surface becomes uneven. Figure 1 shows how this unevenness or topography is developed.

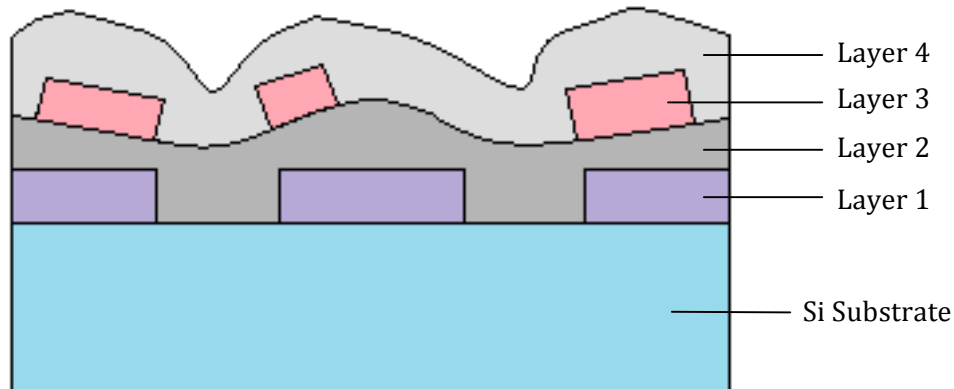


Figure 1 Schematic diagram of surface topography buildup without planarization—
Layer 1: Deposited then etched; Layer 2: Deposited without following planarization
(some topography formed); Layer 3: Deposited and patterned; Layer 4: Deposited
(More topography formed than Layer 2)

During the fabrication process, there is a step called planarization, which is used to decrease the topography of the surface before photolithography (R. Doering et al., 2000). As shown in Figure 1, the unevenness increases and propagates from the bottom layer to the top layer if no planarization step is

included. This buildup of topography is disadvantageous for the photolithographic step because it reduces the accuracy of the pattern transferred from the mask to the photoresist. The reason behind this is that the higher the surface roughness, the wider the distribution of focusing accuracy. Therefore the step height of the surface is restricted by the depth of focus in lithography, which is determined by the wavelength of the light used (H. J. Levinson, 2010),

$$DoF = \frac{k \times \lambda}{NA^2} \quad (1)$$

where DoF is the lithographic depth of focus, k is process-related coefficient, λ is the wavelength of light used, and NA is the numerical aperture of the lens.

Nowadays, the number of transistors per chip has already crossed the line of 40 million and we can expect it to be more than one billion in a decade (J. M. Steigerwald, 1996). Although photolithography is the most advanced technology for nanolithography, as the minimum feature size of the integrated circuits keeps decreasing, sources with smaller wavelengths are used in order to meet the need for higher resolution. A few examples of these nanolithographic technologies are the extreme ultraviolet lithography (H. J. Levinson, 2010 and V. Bakshi, 2005), electron beam lithography (T. Matsuzaka et al., 1999 and M. Altissimo, 2010) and x-ray lithography (D. Atwood, 1999). These next-generation lithographic technologies (K. Hosono, 2010) are capable of overcoming the diffraction limit of traditional optical lithography. However, this decrease in wavelength reduces the depth of focus. In order to focus the light on wafer surface accurately, a more planar surface is desired. As the packing density of transistors within a chip increases and the signal processing delay needs to be diminished, multilevel metallization for wiring the transistors into a circuit is the prevalently used way in semiconductor manufacturing. With ever-increasing levels of metallization, the requirement for planar surface is becoming even more stringent, and planarization is an essential step of semiconductor manufacturing.

Several techniques have been used in surface planarization during integrated circuit fabrication. One of them is the reflow of Borophosphosilicate Glass (BPSG), which is silicon dioxide heavily doped with boron and phosphorous. The deposited BPSG on the surface reflows during a high temperature anneal, reducing the surface topography slightly. An alternative is the Spin-On Glass (SOG). This technique uses SOG materials, i.e. a liquid silicon oxide precursor, to smooth the wafer surface. The surface is cured at a high temperature in order to evaporate the solvent, and a layer of solid silicon oxide is formed. This dielectric oxide has poor quality compared to CVD and thermal silicon dioxide. These two techniques only achieve local planarization. Both of them involve high temperature treatments, which can increase the chance of impurities diffusing into the silicon layer. Other techniques include the re-sputtering of deposited materials, sacrificial etching and so on. However, they also have big limitations. Etching planarization offers little control of the etching at different locations of the surface. Re-sputtering the deposited materials may damage the device.

In the 1980s, IBM developed a new planarization technique, Chemical Mechanical Planarization. Chemical Mechanical Polishing or Planarization, known as CMP, is a global planarization technique that combines mechanical forces and chemical etching for enhanced polishing and finishing. Pure mechanical polishing produces very rugged surfaces, while chemical erosion is incapable of generate polishing effects but softens the surface. A combination of the two factors makes Chemical Mechanical Polishing a good candidate for global planarization techniques. This planarization process reduces the surface topography to meet the requirements imposed by decreasing lithographic depth of focus with increasing resolution (H. J. Levinson, 2010), with reducing minimum feature size and ever increasing transistor density of Integrated Circuits (IC).

1.2 CHEMICAL MECHANICAL POLISHING

1.2.1 General Review of CMP

Since the introduction of CMP by IBM in the 1980s, many technology business corporations and laboratories have been actively involved in the study and improvements of such technique. The mechanism of this technique is shown in Figure 2a. The wafer to be polished is held upside down by a containing ring beneath a rotating wafer carrier. The carrier applies certain down force on the wafer onto a rotating polishing pad, while simultaneously chemical slurries typically containing abrasive particles and surfactants are replenished to the pad and conditioned by a polishing conditioner. The wafer is rinsed by water after the polishing is finished. Figure 2b illustrates the contact mechanism between polishing pad, abrasive particles (orange dots) of slurries and the wafer surface being polished.

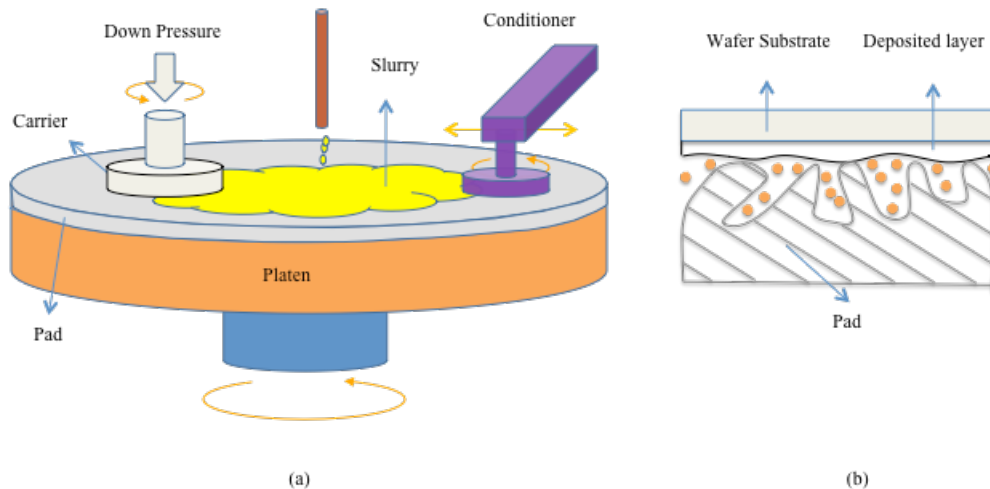


Figure 2 (a) schematic diagram of CMP process, (b) contact mechanism

Chemical Mechanical Polishing is a complex process that is associated with mechanical forces and chemical reactions. Therefore, the results of CMP are mainly determined by the chemical and mechanical factors reported by many publications such as works by (J. P. Abiade, 2004), (Y. Li, 2007) and (U. Paik et al., 2009). The variables that affect the results of CMP include mechanical

properties and conditioning of the polishing pad, process parameters, slurry chemistry, and the properties of surface to be polished. The results of CMP are evaluated by material removal rates, polishing selectivity, Within Wafer Non-Uniformity (WIWNU), Within Die Non-Uniformity (WIDNU) and surface defectivity. A few key factors are the characteristics and chemistry of slurries used in CMP, such as slurry pH, chemical additives, abrasive particle type, size, concentration and morphology. These factors are known to significantly affect the results of CMP (M. Krishnan et al., 2010). The following Figure 3 outlines the input variables and outcome of Chemical Mechanical Polishing.

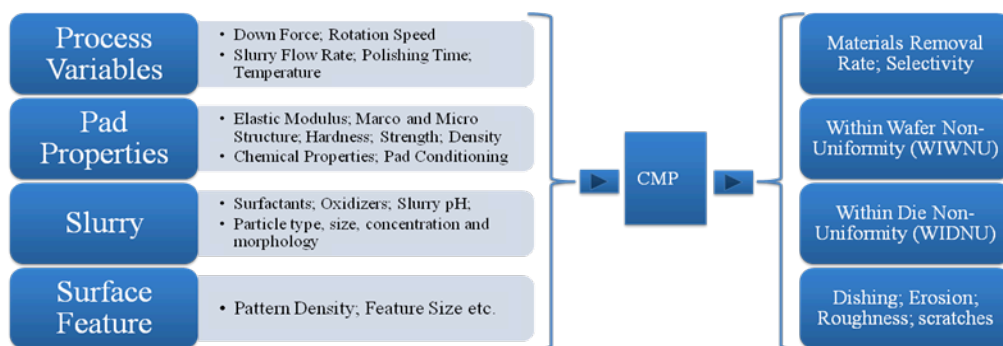


Figure 3 Input (Left) and output (Right) of Chemical Mechanical Polishing

1.2.2 Advantages and Disadvantages of CMP

Chemical Mechanical Planarization offers many advantages comparing to other planarization technologies. The first and foremost advantage of Chemical Mechanical Polishing is its ability of achieving global planarization across the wafer surface. This advantage allows for the semiconductor manufacturing expanding from 4-inch wafers to 18-inch wafers, reducing the cost and improving the throughput (S. W. Jones, 2005). CMP is also capable of polishing multi-material surfaces during the same polishing step, removing severe topography easily to allow higher-density integrated circuit patterns, and higher level of metallization. Since CMP is a subtractive process, it can reduce the surface defects and yield a high quality surface finish. CMP is an alternative method of patterning metals and alloys that are used for wiring the

integrated circuits, such as Chemical Mechanical Polishing of copper and tungsten. Metals are usually difficult to etch, and etching is a destructive process. CMP provides an alternative for metal surface planarization. Many studies have reported on the planarization of metals. The over-filled copper on top of the insulating layer during a copper dual-damascene process is removed in a copper CMP process (S. P. Muraka, 2000; M. R. Oliver, 2003). Tungsten is used in the multilevel metallization since the deposition of tungsten is a good way to fill the vias and plugs that link the successive conductive layers (F. B Kaufman et al., 1991; M. Fayolle et al., 1997; Y.-J. Seo et al., 2005). Tungsten CMP is one of the earliest techniques used in the semiconductor device fabrication, following the oxide CMP. Therefore, CMP is a technique that can be used in the planarization of many different materials. It is also an enabling technology in the fabrication of the next-generation semiconductor devices using new materials and structure designs. In addition, CMP is a safe process, compared to etching (especially dry etching), because it does not involve hazardous gases.

Like every coin has two sides, CMP also has its disadvantages. Firstly, CMP is a relatively new technology of three decades, and the mechanism of exactly how CMP works is still being studied. Therefore, CMP is unable to offer accurate controls of polishing results. Secondly, CMP is a wet process involving friction of abrasive particles, which brings defects such as micro-scratches, particle and ion contamination, dishing and erosion, reducing the die yields. Furthermore, additional processes are needed, such as endpoint detection and post-CMP cleaning. Such additional processes add up the high cost of operations and ownership of CMP from equipment and maintenance to slurry and pad consumables. These disadvantages pose challenges for the future of this technology.

1.2.3 Future and Challenges of CMP

As discussed previously, CMP introduces defects of micro-scratches, particle contamination etc. Therefore, a challenge that CMP faces in future is the reduction of such defects. As the feature size is diminishing, a single abrasive

particle contamination can ruin the function of a whole chip. Moreover, debris worn off from the polishing pad and residues of slurry are bigger particulates, which are an even bigger problem because they cover larger areas of a die. Ions from the slurry that remains inside the device after post-CMP cleaning can affect the performances of the device.

Another challenge of CMP is facing thickness control. Within Wafer Non-Uniformity must be reduced. Although thickness control has been significantly improved by optimizing the conditions of polishing pad, slurry design and distribution, CMP equipment, under-polishing and over-polishing are still seen. Especially in the era of ultra-large-scale integration (ULSI), the ever-decreasing tolerance to wafer surface variations requires dramatic improvements of CMP in thickness control.

The cost of CMP is high, both in capital cost for CMP equipment and in operation cost for CMP maintenance and consumables. The high cost of CMP limits its adoption and can impede its development. Therefore, reducing the cost of CMP is also a great concern for future engineers and researchers.

As new transistors such as the FINFET are seen in the development of today's semiconductors, there is a need for new materials like high-k gate oxide. The future of CMP has to keep pace with this development.

1.3 CMP OF DIELECTRIC MATERIALS

Chemical Mechanical Polishing has been used in the planarization of many different materials, such as metal (Al, Cu, W, Ta, Ti, TiN etc.), dielectric (Silicon, SiO_2 , Si_3N_4 , BPSG, PSG etc.) and other materials. Polysilicon CMP is also found in the MEMS fabrication (J. J. Sniegowski, 1996; B. D. Tang, 2004). In this section, the CMP of dielectric materials are discussed.

1.3.1 Isolation Techniques: LOCOS & STI

Traditionally, local oxidation of silicon, known as LOCOS, is the technique used to isolate adjacent transistors. Figure 4 shows the process flow of LOCOS.

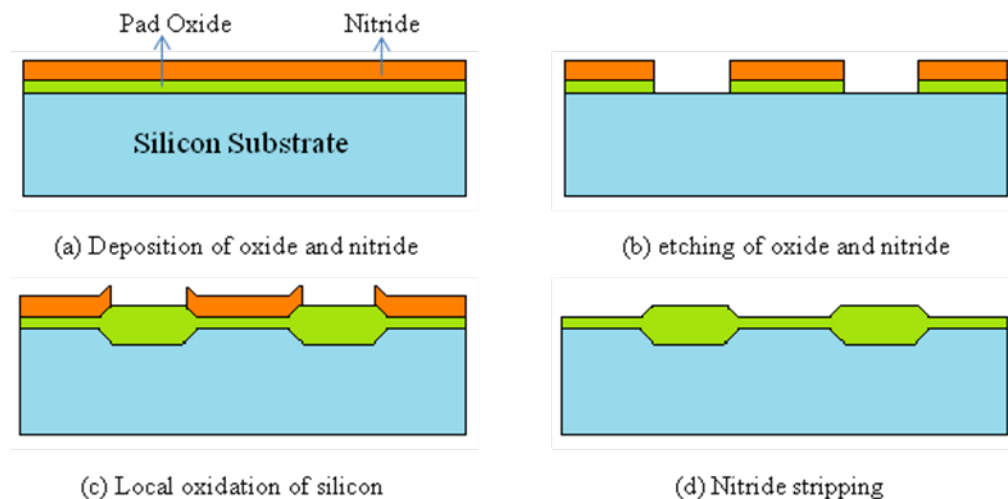


Figure 4 Local Oxidation of Silicon Process

Firstly, a thin layer of pad oxide is deposited on the silicon substrate followed by the deposition of a layer of silicon nitride. Certain regions of these two layers are then etched, where the thermal oxide will be grown. Such thermal oxide can grow into the silicon substrate so it can insulate the transistors. Etching field oxide is not a way for isolation because it is deposited above the silicon substrate. After the local oxidation process is finished, the silicon

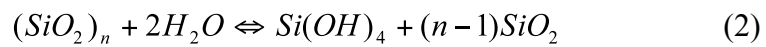
nitride layer that was used as a mask to prevent to the growth of thermal oxide in the active regions of transistors is stripped.

As the size of ICs is reduced, this conventional isolation technique needs to be replaced due to the undesirable “bird’s beak”. In the case of semiconductor devices with line widths less than 250 nm, a relatively new process called Shallow Trench Isolation (STI) is required. STI provides good embedding of field oxide into silicon and clear distinction between oxide and active-area regions (Y. Li, 2007) and prevents the “bird’s beak” resulting from lateral encroachment (A. Bryant et al., 1994) of oxide into the active area below the nitride. The improved control over the geometry of the isolated area by STI allows narrow pitches and thus high packing density. A typical fabrication process for Shallow Trench Isolation starts from growing a layer of pad oxide and then depositing a nitride layer on a silicon wafer. A shallow trench is then etched into the silicon substrate, after which liner oxidation and CVD oxide gap fill are conducted to isolate the active regions. Finally, the step of Chemical Mechanical Planarization (CMP) is included to remove the overburden field oxide, and the protective nitride layer is stripped off afterwards.

1.3.2 Interlayer Dielectric CMP

Interlayer dielectric (ILD) materials are used to separate the wiring that connects the transistors. The step height caused by the deposition of such materials needs to be removed to meet the requirement posed by lithographic depth of focus. Chemical Mechanical Polishing is one of the methods. ILD CMP is the earliest example of the utilization of such technology. Many factors affect the CMP of interlayer dielectric materials. Since the theme of this thesis is about the slurry, the characteristics of the slurries used in polishing are reviewed.

Fumed or colloidal silica particles are widely adapted in CMP of Interlayer Dielectric (ILD) materials, poly-silicon and metal mainly due to their affordability and good colloidal stability. Extensive studies on ILD CMP using silica have been conducted (J. Kim et al., 2002 etc). ILD CMP is a mechanical dominated process. Usually the CMP of ILD materials, i.e. silicon dioxide, is conducted at pH around 10 with considerably high abrasive concentrations. At an alkaline pH, the silicon dioxide surface goes through a hydrolysis reaction to form a soft layer of Si-OH groups under tensile stress (M. Krishnan et al. 2010),



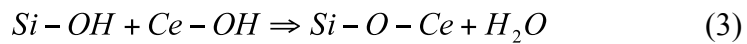
Such a soft layer is favored for high oxide removal rates. Therefore, ILD CMP is usually done at alkaline pH and under fairly high down pressure.

1.3.3 Shallow Trench Isolation CMP

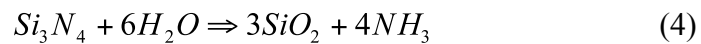
The reason why Shallow Trench Isolation is used was discussed previously. In the Chemical Mechanical Polishing for Shallow Trench Isolation, the polishing process should have a good oxide polishing rate in order to reduce the cost of operations, and meanwhile it should be able to stop by itself at the protective nitride layer beneath the oxide. Therefore, selectivity between oxide and nitride in STI CMP is desired.

Two major types of slurries, silica-based and ceria-based, are used in STI CMP. The conventional silica-based slurry for STI CMP usually provides relatively low selectivity of oxide over nitride (R. Manivannan, 2008), which is disadvantageous in polishing endpoint detection. With the decreasing thickness of silicon nitride film beneath field oxide and the feature size, a high oxide-to-nitride selectivity is required to minimize over polishing and defects such as dishing or erosion. In many studies, ceria-based slurries, in comparison, exhibit good polishing selectivity, especially when certain nitride

polishing suppression chemicals are added. The ceria-based slurries are also more effective in oxide polishing from a “per abrasive particle weight” perspective. The improved polishing is attributed to the presence of a chemical reaction between ceria and silicon dioxide film surface in aqueous media, forming a chemical bond of Ce-O-Si. The movement of bonded ceria particles from the bonding sites, caused by mechanical shearing forces from the polishing pad known as the chemical tooth effect proposed by (L. M. Cook, 1990), is responsible for the high oxide removal rate.



The chemical aspect the CMP of silicon nitride involves converting the Si-N bond into Si-O bond, as shown in the following equation,



After the surface modification shown in equation (4), the resulted Si-O bonds further react with H_2O as shown in equation (2), forming the soft layer containing silanol groups. Therefore, a way to reduce the nitride removal rates during STI CMP is to minimize reactions (2) and (4). Studies have shown that by using chemical surfactants that preferably absorb onto silicon nitride surfaces, the nitride polishing rates are significantly decreased.

1.3.4 Mixed Abrasive Slurries for STI CMP

Slurries with mixed abrasives are not commonly seen, especially in STI CMP. Lu et al. (2003) reported that the polishing rates and surface qualities of thermal oxides using mixed slurries of ceria and silica were better than those using single component, silica or ceria, based abrasive slurries. In the study of Kim et al. (2006), ceria-coated silica slurries were prepared by the hydrothermal reaction of ceria and silica nanoparticles after mixing them together. The CMP polishing efficiency of such slurries was presented.

However, there was no systematic comparison of its polishing performances. Lee et al. (2002) also published similar study on ceria-coated silica slurries for CMP through heat treatment. Babu and his group (2003) reported mixed-abrasive slurries made of two kinds of particles: alumina and silica. Their study showed a dramatic improvement in the oxide removal rate. With use of these kind of mixed abrasive slurries, the selectivity between oxide and nitride films was reported to be as high as 65, while the surface roughness was further reduced. To the best of our knowledge there are few studies on CMP by mixed ceria and silica slurries or the stability of such slurries. None of the previously mentioned papers included the colloidal stability of the slurries and its correlation with their CMP efficiency on oxide. Neither did they provide guidance in optimizing the compositions of such mixture of particles in order to achieve higher polishing rates. In addition, most of those studies required complicated preparations of the slurries, which excluded them from potential applications in industry manufacturing, unless a simplified and equivalent way was presented.

The colloidal stability of slurries used in Chemical Mechanical Polishing is an important factor that affects the polishing performances. It may affect the material removal rate; the agglomeration caused by poor stability is believed to be a cause of micro-scratches seen in STI CMP. Therefore, study of the colloidal stability of slurries, the interactions between slurry particles and the interactions between slurry particles and surfaces to be polished, can be very important for both mixed abrasive slurries and slurries with one kind of particle.

1.4 ZETA POTENTIAL (ζ -POTENTIAL)

When a particle is placed inside an aqueous media, it typically acquires some surface charge. This acquisition of charge on particle surface is believed to be from the ionization of particle surface bonding groups and the dipolar attributes of the surface. Under electrostatic attraction, a layer of oppositely charged ions—counter ions--- is formed on the particle surface. The formation of layer is called the stern layer. Further out from the stern layer where the counter ions are strongly attached to the particle, the ions, both counter ions and some co-ions are less strongly bonded to the stern layer. This layer of ions next to the stern layer usually moves with the particle under Brownian motion, and it is called the diffuse layer. A notional outer boundary of the diffuse layer is known as the slipping plane. The two layers are called the electrical double layer, and the electrokinetic potential at the slipping plane is compared to that of the bulk solution. Figure 5 is an illustration of zeta potential of a particle in aqueous media.

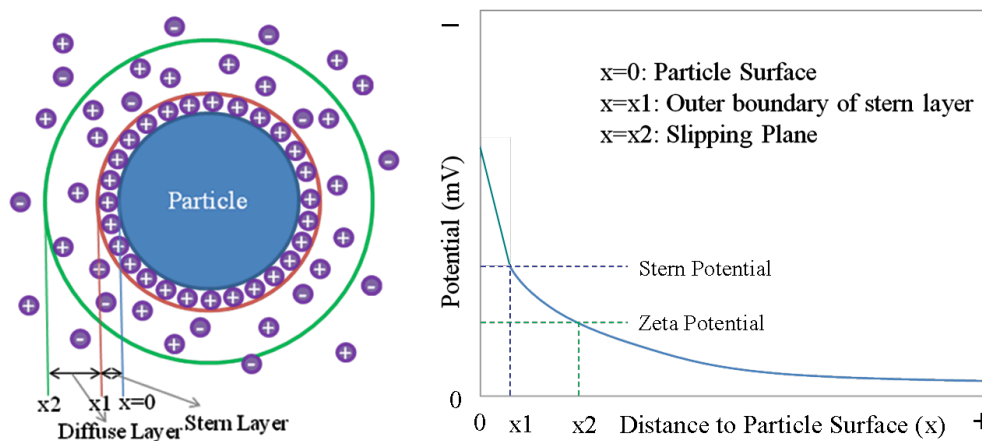


Figure 5 Illustration of electrical double layer and zeta potential

Zeta Potential is a key characteristic of a colloid system, which is usually an indicator of the stability of the colloid. Colloidal suspensions with high zeta potential are very stable because of the electrostatic repulsion force between particles.

1.5 SUMMARY OF INTRODUCTION

To summarize this chapter, the colloidal stability of slurries is an important factor that affects the performance of Chemical Mechanical Polishing. It can be studied through the characterization of the abrasives used in the slurry such as particle size, morphology, zeta potential etc. To date, not many studies have been reported the colloidal stability of mixed abrasive slurries and the correlations between the slurry colloidal stability and its CMP performances. This thesis has focused on the stability of mixed abrasive slurries composed of ceria and colloidal silica nanoparticles, which were prepared by simply adding two kinds of commercially available slurries without any further treatment, and their affect on CMP of PECVD silicon dioxide films. The stability was studied via settling tests and surface charge analysis, and was correlated to CMP performance on oxide thin films.

CHAPTER 2 EXPERIMENTAL PROCEDURES

2.1 MATERIALS & SAMPLES PREPARATION

2.1.1 Materials

Three kinds of silica slurry supplied by Akzonobel, namely Bindzil EB6080 (EB6080), Bindzil EB6040 (EB6080) and Bindzil 40/130 (BZ), and one kind of ceria slurry from Nyacol Nano Technologies, named CEO2(AC), were used in this study. The particle concentrations of the slurries are 35.48 wt%, 38.98 wt%, 42 wt% and 20 wt%, respectively.

The purified de-ionized water, which was prepared by Milli-Q UV PLUS and referred to as Milli-Q water, was used in slurry dilutions and all other occasions as needed. The pH of samples was measured by Accumet Basic AB15 pH meter, which was calibrated each time prior to its use. Unless indicated otherwise, citric acid and potassium hydroxide were used to adjust the pH of samples.

4-inch silicon wafers were used for silicon dioxide and silicon nitride depositions.

2.1.2 Sample Preparation

All the samples and slurries that were used in size measurements, zeta potential measurements, settling tests, TEM and Chemical Mechanical Polishing were prepared in the same way from the dilution of original slurries mentioned in section 2.1.1.

2.2 PARTICLE SIZE DISTRIBUTION

Particle sizes and size distributions of all four slurries were determined using Nano ZS Zetasizer from Malvern Inc. All suspensions used in particle size distribution measurements were prepared by dilution of the original slurries to approximately 0.5 wt%. The pH of the suspensions was adjusted to 4 ± 0.05 . The measurements were conducted at room temperature, 25°C , using a refractive index of 1.457 for silica, 1.33 for water and 2.1 for ceria. The particle size reported was the average of four successive readings of the same suspension (except that ceria had only two readings).

The Malvern Nano ZS Zetasizer applies a non-invasive technique called Dynamic Light Scattering (DLS) to measure the size of particles and molecular aggregates in the submicron range. When the particles inside the suspension are illuminated with a laser, the intensity of the scattered light fluctuates, as a result of Brownian motion, at a rate that is dependent on the size of the particles. Analysis of these light intensity fluctuations yields the velocity of particles due to the Brownian motion, from which the particle size is calculated based on the theory of Brownian motion proposed by A. Einstein (1956):

$$R = \frac{kT}{6\pi\eta D} \quad (5)$$

where, R is the hydrodynamic radius, k is the Boltzmann constant, T is sample temperature, η is the viscosity of the liquid and D is diffusion coefficient.

2.3 ZETA POTENTIAL MEASUREMENTS

Zeta Potential are not measured directly, but it can be calculated from theoretic models and experimentally measurable parameters, such as electrophoretic mobility. Dispersed particles typically have surface charge as described in section 1.4; when a electric field is applied particles within the media will migrate toward the electrode of opposite charge with certain velocity. This velocity is proportional to the magnitude of electric field it is in.

The electrophoretic mobility of this particle under certain conditions is defined as,

$$\mu_e = \frac{v}{E} \quad (6)$$

where v is particle velocity, E is the electric field applied, and μ_e is the electrophoretic mobility of the particle.

In electrophoresis, one well known theoretic model that correlates the electrophoretic mobility and zeta potential of a particle within aqueous media was presented by Smoluchowski in 1903:

$$\mu_e = \frac{\varepsilon_0 \varepsilon_r \zeta}{\eta} \quad (7)$$

where ε_r is the dielectric constant of dispersant, ε_0 is the permittivity of free space, ζ is the zeta potential of the particle and η is the viscosity of the dispersant.

There are a few techniques that can measure the zeta potentials of particles in aqueous solutions. In this study two techniques were used: Malvern Nano ZS Zetasizer and Zetaphoremeter III. The main principles are the same for both techniques The difference is how the electrophoretic mobility is measured.

2.3.1 Malvern Nano ZS Zetasizer

The Malvern Nano ZS Zetasizer measures the electrophoretic mobility through the frequency shift or phase shift of an incident laser beam caused by these moving particles. Such mobility is then converted to zeta potential using equation (7).

The ζ -potentials of silicon dioxide (EB6080), silicon nitride and ceria particles were measured over a wide pH range, using Malvern Nano ZS Zetasizer. The ζ -potentials of MAS samples made from the three silica and ceria slurries were also measured at a few selected pH values. The ζ -potential reported for each sample was the average of three consecutive measurements. The ζ -potential measurements were measured at room temperature (25°C); the refractive

indices used were 1.457 for silica, 1.33 for water, 2.05 for nitride and 2.1 for ceria. The adsorptivity was set to 0.01 for silica and silicon nitride, 0.05 for ceria. The viscosity was set at $8.872 \times 10^{-4} Pa \cdot s$, which is considered to be the same as the viscosity of suspensions. A clear, disposable curvette supplied by the vendor was used as suspension holder. The curvette was rinsed twice with Mill-Q water and then rinsed three times with the sample suspensions to be measured.

2.3.2 Zetaphoremter III (SEPHY/CAD)

The Zetaphoremter III (SEPHY/CAD) measures particle mobility through the analysis of the movement images of particles captured by a build-in video camera. The Zetaphoremter III is equipped with a laser illuminator that generates light to illuminate the particles within solution, a rectangular electrophoresis cell with a pair of hydrogenated palladium electrodes where electric field can be applied, and a digital video image capture (CCD camera) and viewing system. The images captured are analyzed by built-in software, and zeta potential distribution of the particles captured is calculated. The software also gives the average zeta potential and the standard deviation of each measurement. Figure 6 is a photo of Zetaphoremter III.

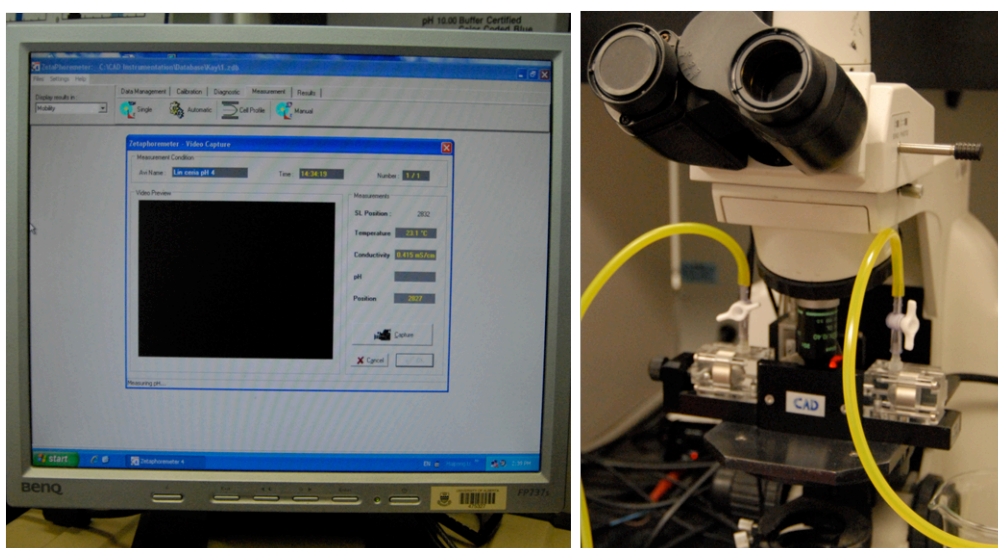


Figure 6 Zetaphoremter III (left: analyzing software; right: measuring system)

The ζ -potential distributions of a few selected samples described above in section 2.3.1 were measured using Zetaphoremeter III (SEPHY/CAD), which was previously used by Liu et al. (2002) in their study of bitumen-clay interactions in aqueous media. Similarly, the captured images of about 20 to 100 particles in the stationary layers of suspensions were analyzed by the built-in image processing software, which generated the distribution histograms of particle electrophoresis mobility and ζ -potential. The environmental temperature was maintained at approximately 22°C. And the viscosity was set to $8.872 \times 10^{-4} Pa \cdot s$.

2.4 SETTLING TESTS OF MIXED ABRASIVE SLURRIES

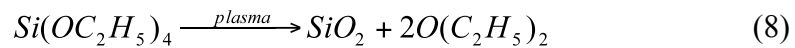
Settling tests of mixed abrasive slurries of silica and ceria colloidal particles were conducted at various ceria to silica weight ratios. Two kinds of silica were mixed with ceria slurry. In the resulting mixtures the weight concentration of silica, either Bindzil EB6080 or Bindzil 40/130, was kept at 5 wt%, while the weight concentration of ceria was varied. The pH of the mixed slurries was adjusted to 4. The mixtures were subjected to simultaneous stirring before the first set of photos was taken. Photographs of all samples were taken using a Nikon D200 under automatic exposure and focusing over a period of several days or weeks. The photographs were not edited except for cropping and proportional resizing.

2.5 TRANSMISSION ELECTRON MICROSCOPY

Transmission Electron Microscopy of silica (EB6080) particles, ceria particles as well as mixture of ceria and silica (EB6080) particles was carried out using the JOEL 2010 TEM (IaB6 electron gun). The samples were prepared by dropping droplets of pre-made solution of ceria, silica and mixture of silica and ceria at pH 4 respectively on carbon-coated copper grids purchased from Ted Pella Inc. The grids placed within wafer carriers were air-dried in a sealed glass desiccator to minimize contaminations for two days before the images were taken.

2.6 PLASMA ENHANCED CVD (PECVD)

The PECVD, Plasma Enhanced Chemical Vapor Deposition of silicon dioxide and silicon nitride was carried out using a Trion PECVD system at 300 °C. TEOS (Tetraethyl Orthosilicate) was used for the deposition of oxide,



And silicon nitride,



The thickness after depositions was around 1200 nm for oxide and 500 nm for nitride for all depositions.

2.7 CMP WITH MIXED ABRASIVE SLURRIES

Polishing was carried out on an Axis 372M polisher. The oxide thin films were polished for 1.5 minutes under 4 psi down pressure and a relative velocity of 0.89 m/s between the wafer and polishing pad. The slurries were constantly mixed at 450 rpm using a magnetic stir while they were pumped onto the pad at a rate of 100 ml/min. These parameters are outlined in Table 1. They were the same for all polishing conducted unless indicated otherwise.

The thickness of oxide were measured prior to and after each polishing, using a Filmetrics resist and dielectric thickness mapping system. The oxide polishing rates were calculated by dividing the change of thickness with polishing time.

Table 1 Process parameters used in Chemical Mechanical Polishing of Oxide

Process Parameters Set for Chemical Mechanical Polishing	
PREWET	Platen speed: 30rpm; Slurry flow: 200 ml/min
PHASE I	Platen/Carrier speed: 50rpm/50rpm; Slurry flow: 100ml/min; Down pressure: 4.0psi; RINSE OFF
PHASE II	Platen/Carrier speed: 30rpm/80rpm; RINSE ON

CHAPTER 3 RESULTS AND DISCUSSIONS

3.1 PARTICLE SIZES

Figure 7 is screen captures of particle size distribution by intensity for the four slurries. The four individual lines for each of the three silica slurries represent the four repeating measurements conducted.

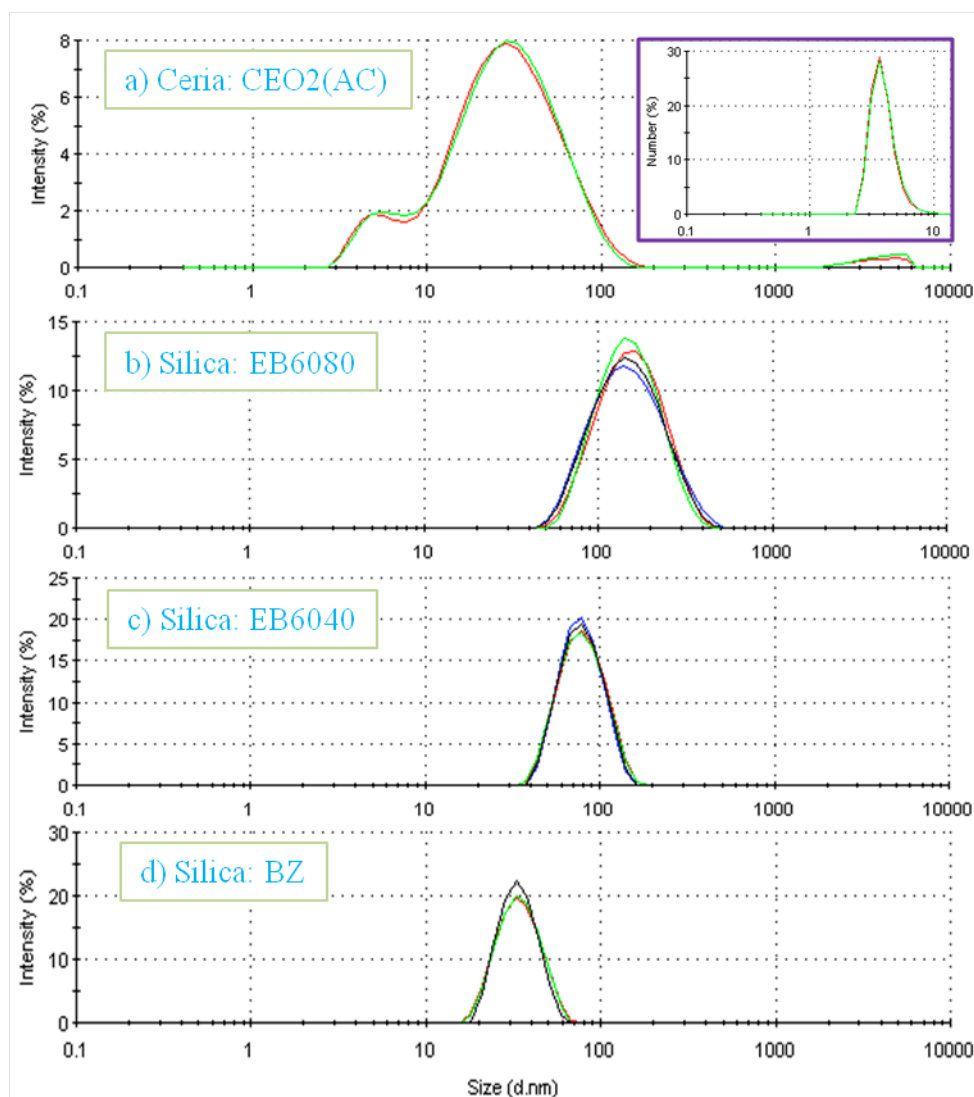


Figure 7 Screen Captures of Particle Size Distributions by intensity (%) at pH 4—a) Ceria Slurry; b) Silica EB6080; c) Silica EB6040; d) Silica BZ

Note: Inserted graph in Figure 7 a) is ceria size distribution by Number (%)

Figure 7 shows that the ceria particles are of bimodal particle size distribution with a primary size of about 5.4 nm and a secondary size of about 35 nm. The

bimodal distribution is probably a result of particle agglomeration. The primary size of ceria particles in this measurement is consistent with the value provided by particle supplier, 5 nm. The inserted graph in Figure 7a, which is the PSD of ceria by number, appears mono-disperse and indicates a low degree of agglomeration. Therefore, it is believed that the majority of the particles within ceria slurries have particle sizes that are close to 5 nm. On the other hand, each of the three silica slurries exhibited its own mono-dispersed behavior. EB6080 had the largest average size and BZ had the smallest for silica particles. The sizes are outlined in Table 2.

Table 2 Particle sizes of silica and ceria (5.44 nm is the primary size of ceria)

Slurry	Sample Conc.	Sample pH	Average particle size
EB6080	0.5 wt%	4	132.2 nm
EB6040	0.5 wt%	4	75.1 nm
BZ	0.5 wt%	4	32.5 nm
CEO2(AC)	0.5 wt%	4	5.44 nm

3.2 ZETA POTENTIALS & SETTLING TESTS RESULTS

3.2.1 Zeta Potentials of Individual Particles

For measurements of the average ζ -potentials separately, the silica (EB6080) and ceria suspensions were prepared to a concentration of approximately 0.5 wt%. Nitride suspensions were prepared by adding a desired amount of nitride

nano powder (Sigma Aldrich) to Milli-Q water to a particle concentration of approximately 0.01 wt%. The ζ -potential was measured by applying an electric field across the sample suspension, using Malvern Nano ZS Zetasizer. Figure 8 shows the ζ -potentials of silica, ceria and nitride at various pH values. The three lines in Figure 8 represent the trend-lines of measurement results for silica, ceria and silicon nitride particles.

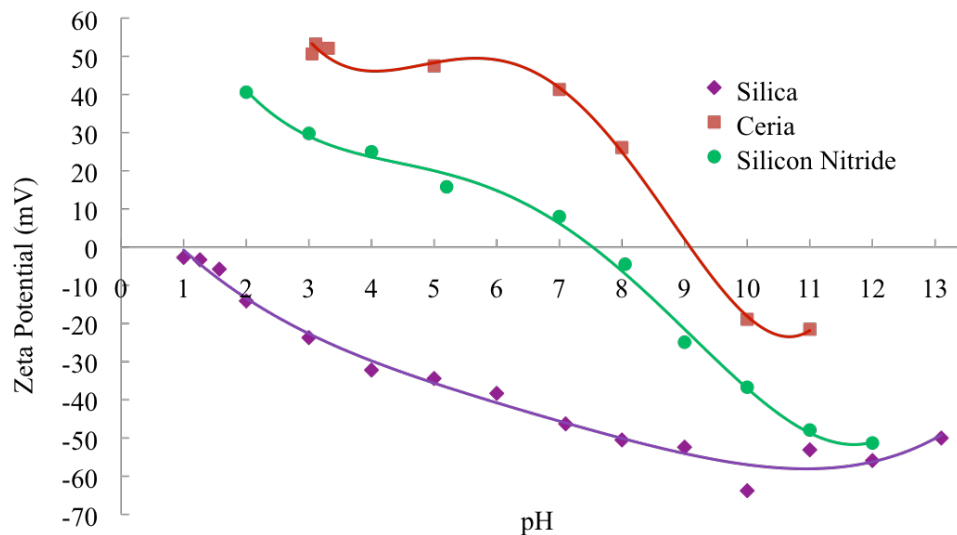


Figure 8 ζ -potential of silica (EB6080), silicon nitride and ceria particles

Figure 8 shows the variation of ζ -potential of silica, ceria and nitride suspensions as a function of suspension pH values. It is evident that silica has negative ζ -potentials over the entire pH range from 1 to 13. In contrast, ceria and silicon nitride suspensions have an iso-electric point at pH approximately 9 and 7.5, respectively. To take the advantage of the chemical tooth effect of ceria in oxide polishing (L. M. Cook, 1990), ceria particles are expected to be attracted to the oxide surface and expelled by the nitride surface by controlling their surface charge. Mixed abrasive slurries of ceria particles and silica particles can be prepared over a pH range of 3 to 8. Over this pH range, ceria particles are expected to attach to silica particles in the mixture due to electrostatic attraction, making the ceria-coated silica particles positively charged when ceria concentration exceeds certain values. The positively charged composite particles are expected to be expelled by similarly charged

nitride surface over the same pH range. Therefore, a pH range of 3 to 8 is likely to be desired for STI chemical mechanical polishing.

3.2.2 Initial Settling Tests of Mixed Abrasive Slurries

According to Figure 8, when ceria and silica particles are oppositely charged, they are supposed to be attracted to each other due to electrostatic attraction when they are mixed together. The attachment of ceria particles to silica particles may result in changes in the ζ -potential of ceria-coated silica and thus the stability of the resulted mixed abrasive slurry. This was partly confirmed by the results of a settling test shown in Figure 9. The silica (EB6080) concentration of the slurry suspensions for the settling was 5 wt% while the ceria concentrations were 1 wt%, 2.5 wt%, 5 wt%, 8 wt% and 16 wt% respectively.

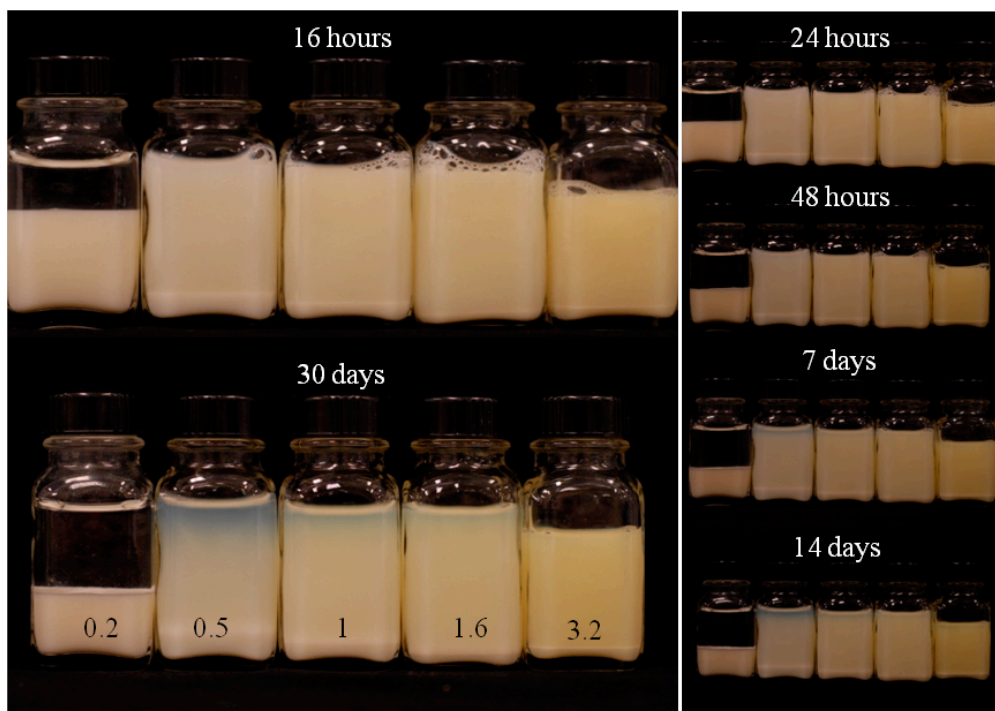


Figure 9 Settling of mixed abrasive slurries at pH 4 ceria to silica weight ratio (left to right): 0.2, 0.5, 1, 1.6 and 3.2 (silica EB6080 5wt%)

In Figure 9, the number at the bottom of each bottle indicates the weight concentration of ceria (wt%) inside the corresponding suspension. The settling of 5 wt% silica slurry was also investigated and it showed a good stability over long period (not shown here) because of its fairly high negative ζ -

potential at pH 4 (Figure 8). From the progress of settling for each suspension shown in Figure 9, it is clear that at a ceria concentration of about 1 wt%, the settling was much faster than the other suspensions, indicating a much lower ζ -potential at this ceria concentration. As the ceria concentration increases, the slurry regained stability and the amount of the precipitation at the bottom of suspension bottle decreased. This phenomenon resulted from higher ζ -potential caused by higher concentration of ceria. Therefore, it seemed necessary to investigate the stability and ζ -potential of mixed abrasive slurries with ceria-to-silica weight ratio around 1:5. This was studied and will be shown later.

3.2.3 Model Proposal Based On Zero Net Surface Charge

The transition in stability by adding ceria particles to colloidal silica as described above suggests that a zero net surface charge and ζ -potential can be reached at certain ceria-to-silica weight ratio when ceria and silica particles are oppositely charged. At a given pH in the region where the ceria is positively charged and silica negatively, a number of ceria particles are required to cover silica surface in order to reach overall zero net surface charge. Since smaller particles have a higher surface area to volume ratio than larger particles, the surface area of silica increases as its particle size decreases, given the same weight of silica. This can be shown mathematically. By assuming that the surface charge density varies linearly with ζ -potential (A. S. Dukhin et al., 2002) and that all particles are spherical and of the same size, when the net surface charge is zero, we get

$$S_s \times SCD_s + S_c \times SCD_c = 0 \quad (10)$$

where,

$$\text{Surface area of silica } S_s = N_s \times 4\pi R_s^2 = \frac{3 \times WT_s}{\rho_s \times R_s} \quad (11)$$

$$\text{Surface area of ceria } S_c = N_c \times 4\pi R_c^2 = \frac{3 \times WT_c}{\rho_c \times R_c} \quad (12)$$

$$\text{Surface charge density of silica } SCD_s = k_s \times Zeta_s \quad (13)$$

$$\text{Surface charge density of ceria } SCD_c = k_c \times Zeta_c \quad (14)$$

and WT is the weight of particles, ρ is density of particles, R is the radius, k is the geometric factor that relates ζ -potential and surface charge density, $Zeta$ is the ζ -potential of particles at the given pH.

Substituting equations (11-14) into equation (10) we get

$$\frac{WT_c}{WT_s} = -\frac{k_s}{k_c} \times \frac{Zeta_s}{Zeta_c} \times \frac{\rho_c}{\rho_s} \times \frac{R_c}{R_s} \quad (15)$$

According to equation (15), the weight ratio of ceria over silica, at which zero net surface charge is reached, is dependent on the ζ -potentials and sizes of the particles. This weight ratio is called the iso-electric point (IEP) of weight ratio. If the silica particle size is decreased while the ceria particle size remains the same, an increase in iso-electric point of weight ratio is expected. Precisely, if ceria particles and silica particles (EB6080) are mixed together with a pH of 4, when the net surface charge is zero, the weight ratio is estimated to be approximately

$$\frac{WT_c}{WT_s} = -\frac{-29mV}{45mV} \times \frac{7.65}{2.648} \times \frac{5.4nm}{132.2nm} = 0.076$$

where, $\rho_c = 7.65g/cm^3$, $\rho_s = 2.648g/cm^3$, $2R_s = 132.2nm$ and $2R_c = 5.4nm$, ζ -potentials of silica and ceria are from Figure 8, and $\frac{k_s}{k_c}$ is assumed to be 1. In

this calculation, the primary size of ceria particles, 5.4 nm, was used instead of its average size, 20.39 nm. There are several considerations attributed to this.

Firstly, the agglomeration of ceria particles, as indicated by the PSD by intensity in Figure 7, was believed to be negligible since the ceria PSD by number was mono-disperse as discussed previously. The relatively higher peak at the secondary size than that at the primary size was attributed to the fact that larger size particles reflect light much more effectively.

Secondly, at pH 4, the ceria has a high ζ -potential of approximately +45 mV as shown in Figure 8, which also supports the assumption that the degree of

agglomeration is negligible. In addition, the agglomeration of ceria particles is believed to be loose due to the repulsive forces within the agglomeration, and the larger size (secondary size) ceria particles are likely to break apart into primary size easily during polishing due to high shear force. This assumption is backed by the result that the polishing rate of oxide was near zero when using slurry containing ceria particles alone at pH 4. The primary size ceria particles are too small to generate high oxide polishing rates even at ceria concentration as high as 20 wt%. Therefore, one can view the ceria slurry as if it were mono-dispersed with an average size of 5.4 nm, and the weight of ceria attached to silica is approximate to the weight of ceria added (with some negligible amount of larger ceria particles not attached) when net surface charge reaches zero.

3.2.4 Verification of Model

To verify the above estimation of weight ratio at which the net surface charge reaches zero at pH 4 for ceria and silica (EB6080), and the expected increase in iso-electric point of weight ratio as described earlier from equation (15), the effect of ceria addition to silica slurries (EB6080, EB6040 and BZ) on ζ -potential was studied. For the ζ -potential measurements using the Malvern Nano ZS Zetasizer, the silica was fixed at 0.5 wt% for all samples, and the ceria varied from 0.01 wt% to 0.15 wt%. Since the concentration of ceria was relatively low, it was assumed the refractive index of silica was not affected by the addition of ceria. A few tests showed that there was no change in the ζ -potential measurement results for the same mixed slurry sample, such as slurry with 0.5 wt% Silica (EB6080) and 0.15 wt% Ceria, when the refractive index was changed from 1.45 of silica to 2.1 of ceria. The ζ -potentials for these mixtures are shown in Figure 10 (data of ceria with EB6040 not shown).

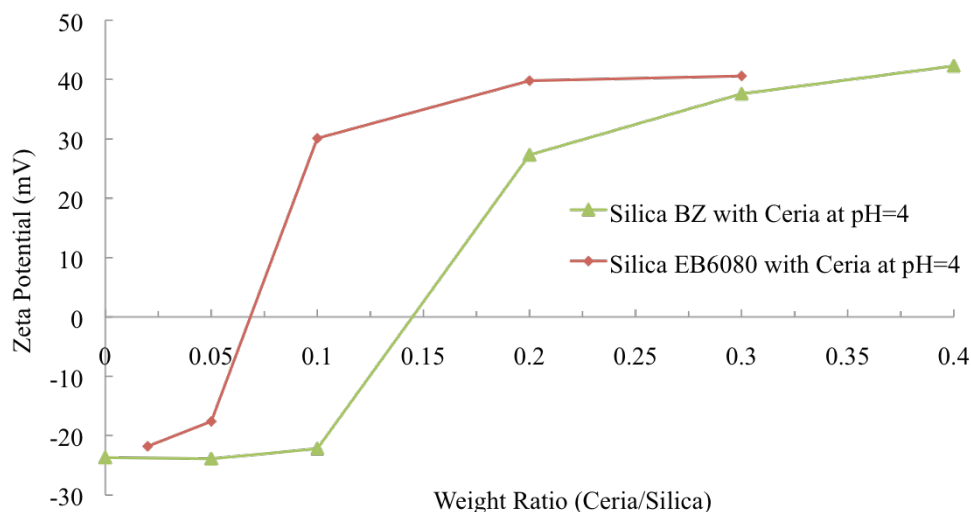


Figure 10 effect of silica (0.5 wt %) particle size on the transition range at pH 4

In case of ceria with silica EB6080 at pH 4, it shows a transition of the ζ -potentials of ceria-coated silica particles over a ceria to silica weight ratio range of approximately 0.05 to 0.1. This range is defined as the transition range (of ceria-to-silica weight ratio).

At about ceria to silica weight ratio of 0.067, the zeta potential of such mixture was zero. This agrees well with the value of iso-electric point of weight ratio calculated from equation (15), 0.076. Outside of the transition range of 0.05 to 0.2, the ζ -potentials of the particles were relatively high. While within this range, the suspension is expected to be unstable and precipitate quickly due to lower ζ -potentials. As the ceria to silica weight ratio exceeded 0.2 wt%, the ζ -potential leveled off at a value of about +40 mV, which was approximately the same value as the ceria ζ -potential at pH of 4 as shown in Figure 8. This transition in ζ -potential was believed to be due to the attachment of positive ceria particles to the silica surfaces, reducing the overall net silica charge from negative to zero as discussed in the model. As ceria concentration was further increased, the net silica surface charge increased from zero to a positive value slightly lower than the ceria ζ -potential.

In case of ceria with silica BZ, compared to that of ceria with silica EB6080, a substantial shift in zero zeta potential weight ratio, in other terms, iso-electric point of weight ratio to a higher value was seen in figure 10. This was due to a

significant increase of silica surface area as the silica particle size decreases from 132.2 nm (EB6080) to 32.5 nm (BZ). The iso-electric point of weight ratio for slurry with EB6040 and ceria was slightly larger than that of slurry with EB6080 and ceria, which is consistent with what the model of equation (15) indicated. The results were not shown in Figure 10.

Figure 11 shows the quantified changes of iso-electric point (IEP) of weight ratios as a function of silica particle sizes/silica surface area. The data of Figure 11 was drawn from the x-intercepts of Figure 10. These changes were successfully predicted by the model presented as equation (15). However, the experimental data deviated from the model derived from equation (15) when the silica particle size was decreased. This was mainly due to the fact that silica particles were not of the same size as assumed, and that the estimation of surface area of smaller silica particles (i.e. BZ) was less accurate than that of larger silica particles (i.e. EB6080).

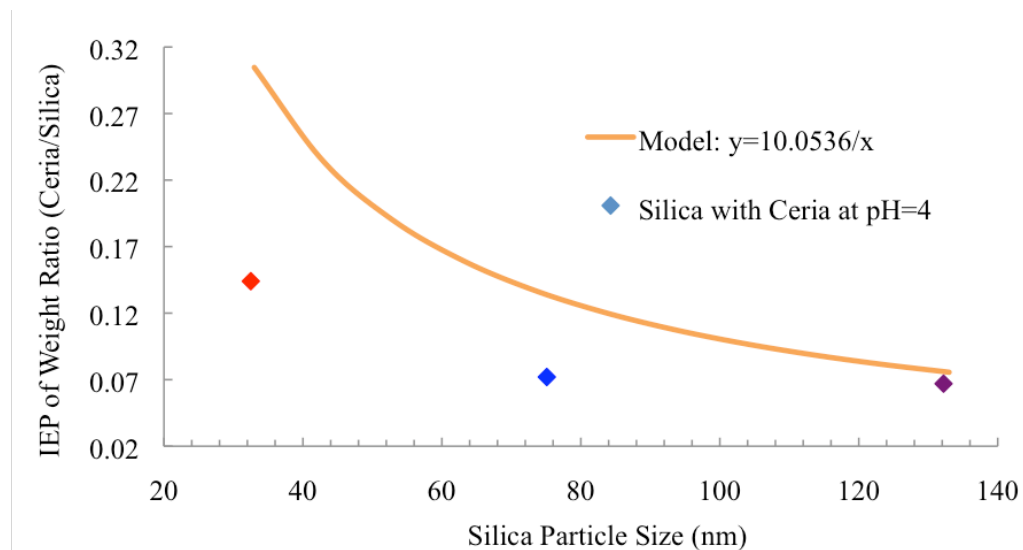


Figure 11 Experimental and Model Iso-Electric Points (IEP) of weight ratio at pH=4 (silica weight 0.5 wt%) as a function of silica particle size (Purple Point: EB6080; Blue Point: EB6040; Red Point: BZ)

In addition, changing the pH the above mixed abrasive slurries should also influence the value of iso-electric point of weight ratio (ceria to silica), as indicated by equation (15). Decreasing the pH from 4 to 3, the iso-electric point of weight ratio decreased from 0.067 to 0.055 according to the zeta

potential results of ceria with EB6080 at pH 3. The results of ceria with silica EB6080 at pH 3 showed similar changes in zeta potential as the ceria to silica weight ratio was increased, therefore they are not shown here. The small shift of iso-electric point of weight ratio from 0.0076 to 0.055 was believed to be due to the changes of zeta potentials of ceria and silica. As the pH changes from 4 to 3, the ζ -potential of ceria particles increases from about +45 mV to +50 mV (see Figure 8), while for silica particles it decreases from about -29 mV to -23 mV. Therefore, to “neutralize” the silica particles at pH 3, it takes fewer ceria particles. This small shift can be also estimated using equation (15).

In case of mixed slurry EB6080 and ceria at pH 3, assuming that $\frac{k_s}{k_c} = 1$,

$$\frac{WT_c}{WT_s} = -\frac{-23mV}{50mV} \times \frac{7.65}{2.648} \times \frac{5.4nm}{132.2nm} = 0.054$$

3.2.5 Zeta Potential Distributions

Since the Malvern Nano ZS Zetasizer gives an average peak value of zeta potential for each measurement, the distribution of zeta potentials for one sample, especially for binary systems like the mixed abrasive slurries in this study, can be very essential and important in evaluating the interactions of silica and ceria particles. In the study of Liu et al. (2002), they investigated the bitumen-clay interactions by the zeta potential distribution measurements at pH 8. The zeta potential distribution obtained from Zetaphoremeter III in their study was essential, since at pH 8 both clay and bitumen were negatively charged (but at quite different magnitude), and therefore an average peak obtained through techniques such as Malvern Nano ZS Zetasizer was insufficient to tell the full story.

However, in this study, silica and ceria particles were oppositely charged at pH 4, and they were supposed to attach to each other in aqueous solution. It was also expected that the zeta potential distributions of such mixed abrasive slurries (binary systems) should exhibit a single peak shifting from the value

of silica zeta potential towards the value of ceria zeta potential as the ceria to silica weight ratio increases from zero when the pH was maintained at 4.

However at pH 10, there should be one peak with a value slightly decreasing (absolute value) from the value of silica zeta potential (at pH 10) as the ceria to silica weight ratio increases, since ceria and silica were both negatively charged and few ceria particles would be attached to silica. In addition, a peak at the value of ceria zeta potential may also be seen. In our case, the results of average zeta potential values obtained at pH 4 from Malvern Nano ZS Zetasizer as shown previously are believed to hold true and informative due to opposite charges of ceria and silica. Nonetheless, it is good to further confirm the validity of the results measured by Malvern Nano ZS Zetasizer and the expectations of zeta potential distributions of the mixed abrasive binary systems at pH 4 and 10.

The zeta potential distribution of silica (EB6080) and ceria were measured separately at pH 4 using Zetaphoremeter III. At various ceria to silica weight ratios from zero to 0.4, the zeta potential distribution of mixed abrasive slurry at each ratio at pH 4 was obtained by adding the results of at least 3 independent measurements. Based on all the data points of the independent measurements, an average value was calculated along with standard deviation. Figure 12 shows the zeta potential distributions of slurries at a few selected ceria to silica weight ratios at pH 4.

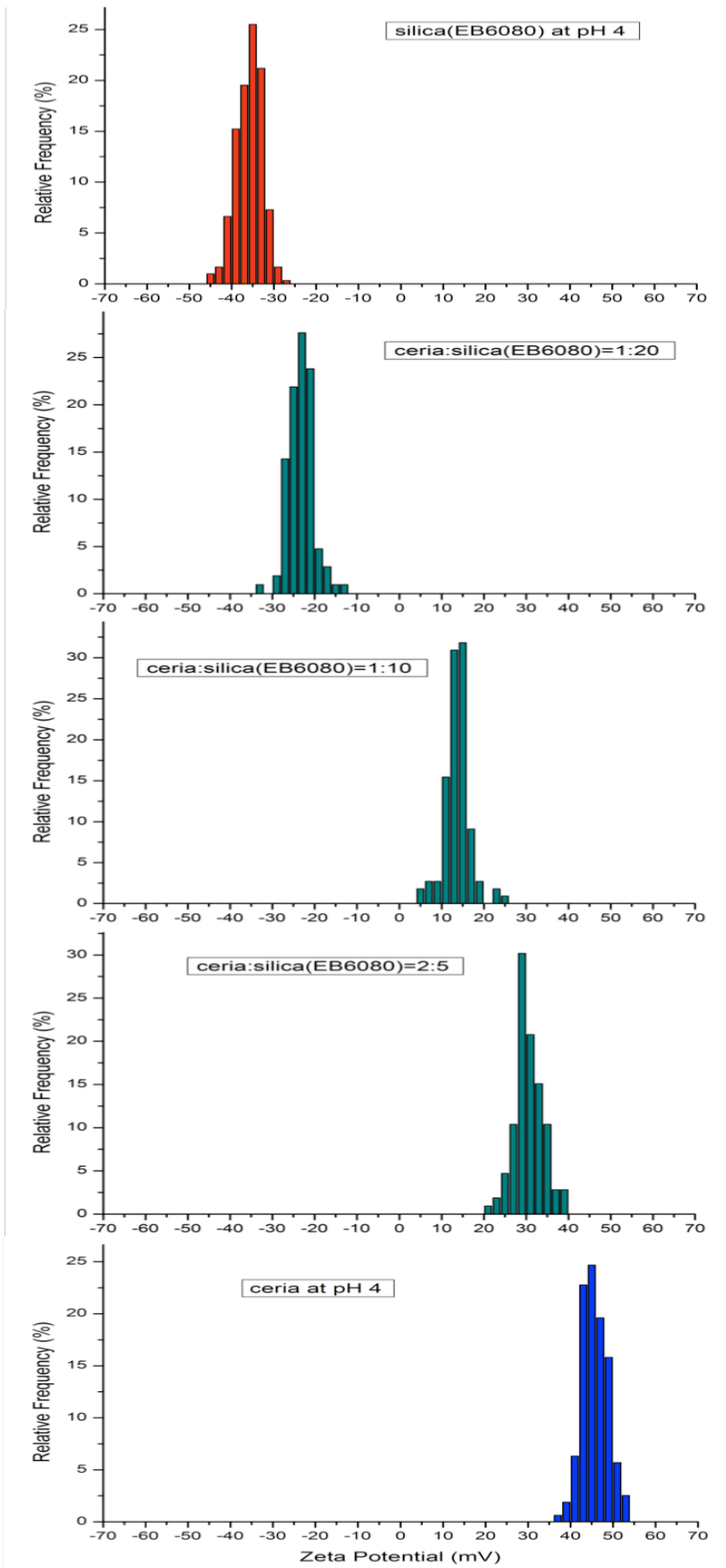


Figure 12 Zeta potential distributions of individual particles (upmost: Silica; bottom-most: Ceria), mixed abrasive slurries at various ceria to silica weight ratios (0.05, 0.1 and 0.4) at pH 4

The average zeta potential of silica at pH 4 using Zetaphoremeter III was -35.8 mV which was close to the value of -32.2 mV using Malvern Nano ZS Zetasizer. For ceria, it was 45.8 mV, which was also very close to the value of about 45 mV given in Figure 8. As the ceria to silica ratio was increased from 0 to 0.05, 0.1 and 0.4 gradually, it is clearly seen in Figure 12 that the single peak of zeta potential distributions shifts towards the peak of ceria alone at pH 4. The results were consistent to the expectations described earlier.

The zeta potential distributions of silica (EB6080) as well as silica (EB6080) with ceria at pH 10 were also measured. The results showed only one peak even high ceria-to silica weight ratio of 0.4. There was no reliable peak seen in any of the mixed abrasive slurries at a value about -20 mV, which was about the average zeta potential of ceria at pH 10 using Zetaphoremeter III. This was due to the fact that the ceria particles (5.4 nm) were much smaller compared to the silica particles (132.2 nm). When they were mixed together and migrated inside the electrophoresis cell of Zetaphoremeter III under applied electric field, the much smaller particles of ceria were out of focus when the larger silica particles were tracked by the image capturing system (CCD camera). Therefore, the zeta distributions only exhibited one single peak even though it was believed that two distinct peaks existed. The work of Liu et al. is a good example of this situation. Figure 13 is the average zeta potential measured by Zetaphoremeter III at pH 4 and 10 using ceria and silica (EB6080) particles, as a function of ceria to silica weight ratios.

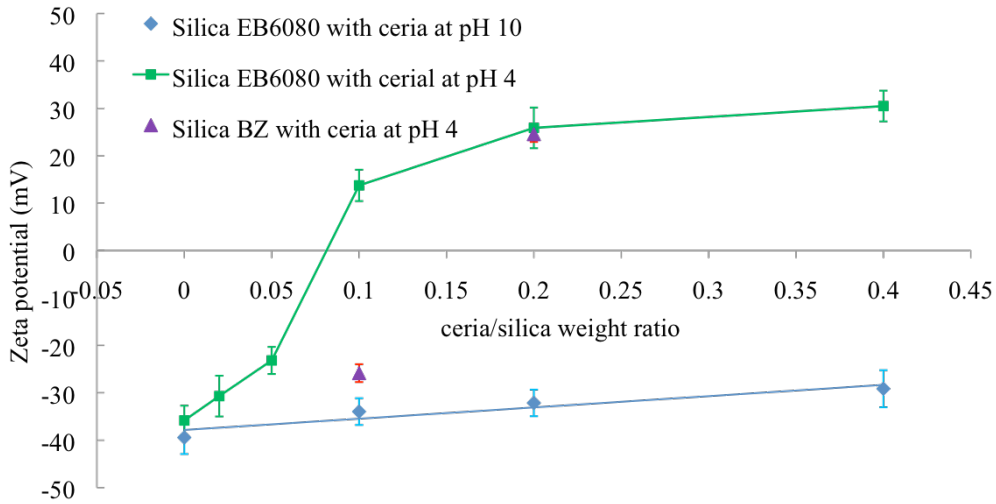


Figure 13 Average zeta potentials of ceria with silica (EB6080—132.2 nm) at pH 4 (square), at pH 10 (circle), and ceria with silica (BZ—32.5 nm) at pH 4 (triangle), using Zetaphoremeter

The data series of ceria with silica (EB6080) at pH 4 has very similar shape as those using Malvern Nano ZS Zetasizer as seen in Figure 10. In fact the iso-electric point of weight ratio in Figure 13 was very close to the value calculated from equation (15) and the value in Figure 10. Not only that, the iso-electric point of weight ratio also had a similar shift in Figure 13 as the silica particle size was decreased. At pH 10, the average zeta potential measured by Zetaphoremter III did not decrease much in absolute value as the ceria to silica weight ratio was increased, indicating few ceria-to-silica attachments at this pH. The shift of zeta potentials at 0.1 (left half of Figure 14) and 0.2 (right half of Figure 14) ceria-to-silica weight ratio, when EB6080 was substituted by BZ, can be visualized in Figure 14.

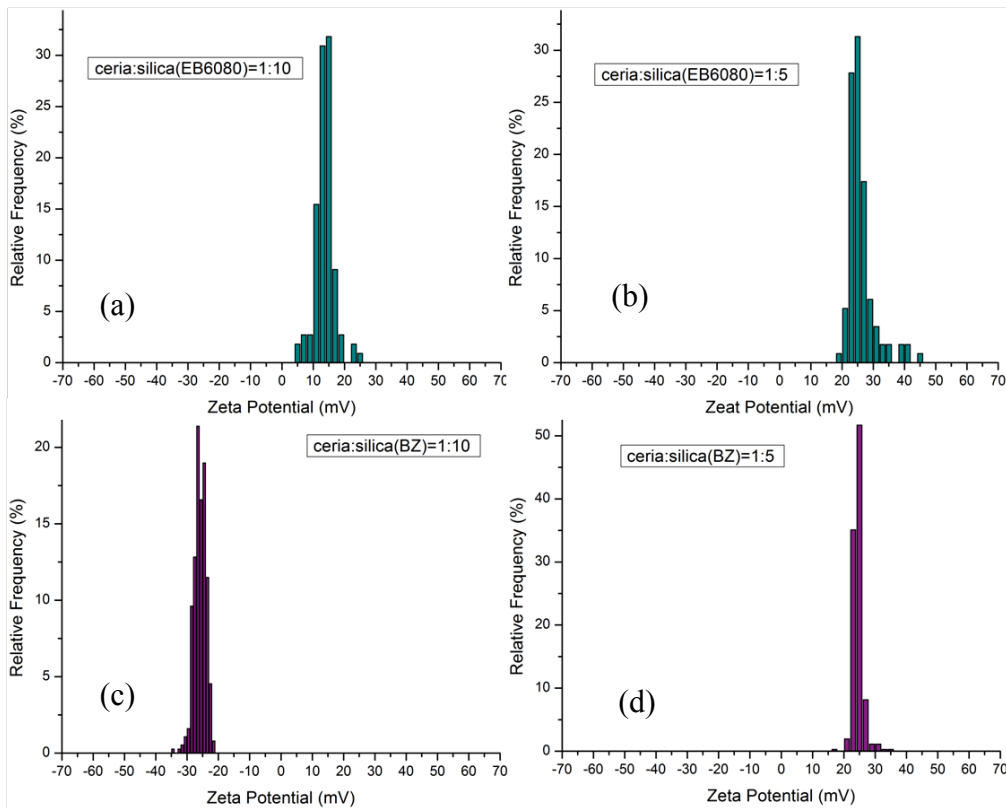


Figure 14 Shift of zeta potential distributions due to change of silica particle size
 (a) & (b) weight ratio of 0.1 and 0.2 for ceria and Silica EB6080
 (c) & (d) weight ratio of 0.1 and 0.2 for ceria and Silica BZ (smaller size)

In conclusion, comparing the zeta potentials measured by the two techniques—Malvern Nano ZS Zetasizer and Zetaphoremeter, the results were in excellent agreement with each other and they validated what was indicated by the equation (15) as we discussed earlier. It should be stressed that the technique of Zetaphoremeter, which gives the zeta potential distributions of samples measured, is a powerful tool to study the interactions of particles/components within a binary or more complicated system. Especially, this technique is very useful when a system is suggested to have a bimodal (or more) zeta potential distribution under the conditions concerned. In contrast, the technique of Malvern Nano ZS Zetasizer, which gives average values (instead of the distribution) of zeta potentials, is not as informative in this case. However, it is capable of providing useful information for single component systems and two-component systems in conditions when a single modal zeta potential distribution is expected, as seen in the case of this study—silica and ceria at pH 4. In addition, it should be noted that there are

limitations of the technique of Zetaphoremter for zeta potential distribution measurements. Based on this study and Liu's work (2002), it is suggested that the technique works best for systems whose components have sizes in the close and relatively high magnitudes. In Liu's study, the clay particles had diameters of about 2 to 4 μm while the particle size of the bitumen emulsion was bimodally distributed with peaks at about 1 μm and 10 μm . Two distinct peaks in zeta potential distributions were seen in the results of some mixture suspensions under certain conditions. However in our study, the silica (EB6080) had an average particle diameter of 132.2 nm and the ceria had an average diameter of 5.4 nm. These two kinds of particles, especially the ceria particles, were much smaller compared to the bitumen and clay in Liu's study. Moreover, the sizes of silica particles and ceria particles were not in close magnitude. Determined by the working principles of Zetaphoremeter, the camera is incapable of capturing images of particles with very different sizes at the same time and under the same focus, neither is it competent in capturing particles of very small sizes since smaller particle deflects less amount of light from the laser illuminator to the camera, resulting in very poor contrasts between the particles and the background. The zeta potential distribution of ceria at pH 4 shown in Figure 12 was a combination of the results of as many as 15 reliable and independent measurements adding together. The reason for such high repetitions was that only a few particles were captured and tracked by the camera in a single measurement due to very small particle sizes. In order to get reliable results, more measurements were conducted in this case. Therefore, both of the two techniques were used in this study.

3.2.6 Stability of Mixed Abrasive Slurries

Similarly as the settling tests shown in Figure 9, settling of mixed abrasive slurries with 5 wt% silica (EB6080) and 0.1 wt%~1.5 wt% ceria were also carried out. The concentrations of silica and ceria within these slurries were higher than those of the suspensions used in zeta potential measurements (Figure 10 and Figure 13), but the ceria to silica weight ratios were the same. Figure 15 shows the settling progress of the mixed abrasive slurries over a period of 72 hours. The number printed at the bottom of each bottle was the ceria to silica weight ratio of the corresponding slurry.

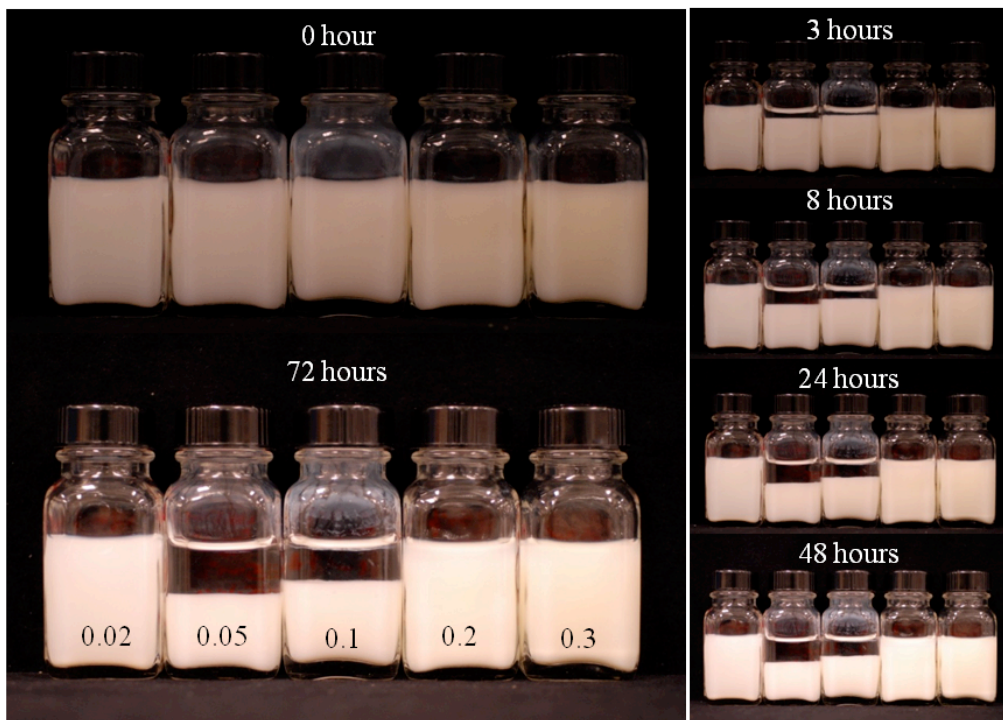


Figure 15 Settling of mixed abrasive slurries at pH 4 (Silica EB6080) ceria to silica weight ratio from left to right: 0.02, 0.05, 0.1, 0.2 and 0.3 (silica 5 wt%)

Comparing Figure 15 with Figures 10 and Figure 13, it is easy to see that the settling results agreed very well with the ζ -potential measurements. A faster precipitation of slurries and higher viscosities were observed at ceria to silica weight ratio of 0.05 and 0.1, indicating lower zeta potentials, which was consistent with the results of Figure 10 and Figure 13. When the ceria concentration decreased from 0.25 wt%, the slurry regained fairly good stability and resembled the settling behavior of 5 wt% silica slurry without addition of ceria. From the two sets of settling tests shown in Figure 9 and Figure 15, a transition of stability occurred at ceria to silica weight ratio between 0.05~0.1 (the transition range as defined in the discussions following Figure 10). The slurry with a weight ratio of 0.2 (1 wt% ceria and 5 wt% silica) in Figure 15, however, precipitated more slowly than the same slurry in the previous settling experiment shown in Figure 9. This may have resulted from a slightly lower ceria concentration in Figure 9, caused by error, and the high sensitivity of slurry stability to ceria to silica weight ratio in the range of 0.05 to ~0.2. The slightly lower ceria concentration caused by error may

explain the “contradiction” of settling behavior for the “same slurry” as was seen in the early stage of settling.

When using silica BZ instead of silica EB6080 for such settling tests at pH 4, it was observed that the rapid settling moved to higher ceria to silica weight ratios, as shown in Figure 16, which also corresponded well with the zeta potential results in Figure 10 and Figure 13. A comparison between Figure 15 and Figure 16 corresponds well with the zeta potentials measurements by both Malvern Nano ZS Zetasizer and Zetarphoremter III.

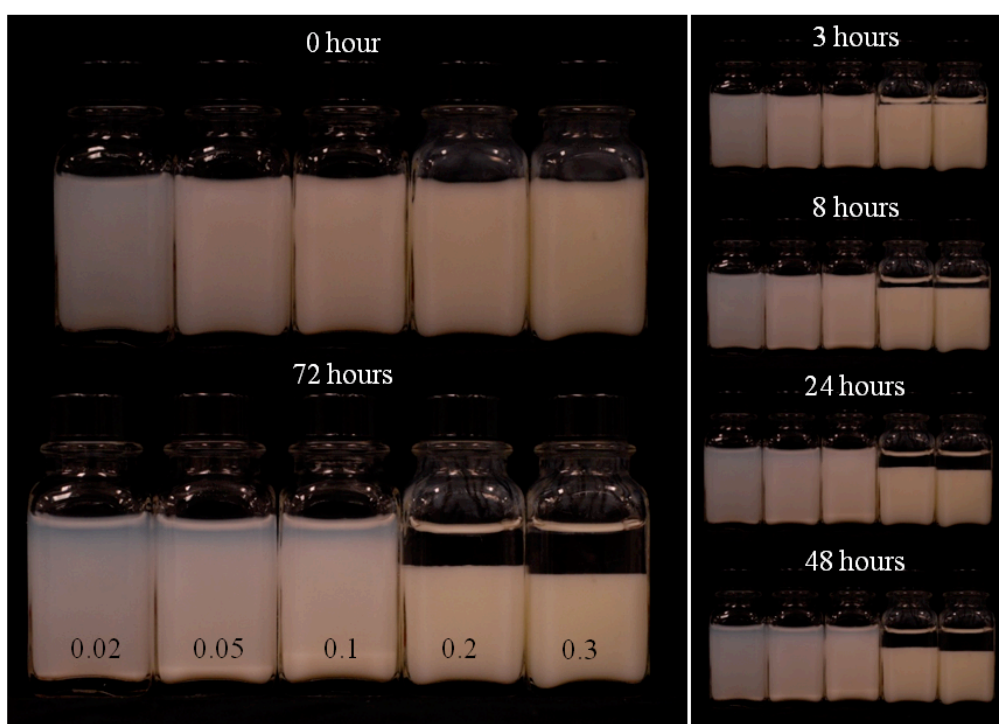


Figure 16 Settling of mixed abrasive slurries at pH 4 (Silica BZ)
ceria to silica weight ratio from left to right: 0.02, 0.05, 0.1, 0.2 and 0.3 (silica 5 wt%)

3.3 TEM RESULTS

3.3.1 TEM of Ceria-Coated Silica Made at pH 4

Figure 17 shows the bright field TEM images of the particles used in zeta potential measurements. All silica particles seen from the TEM images were silica EB6080.

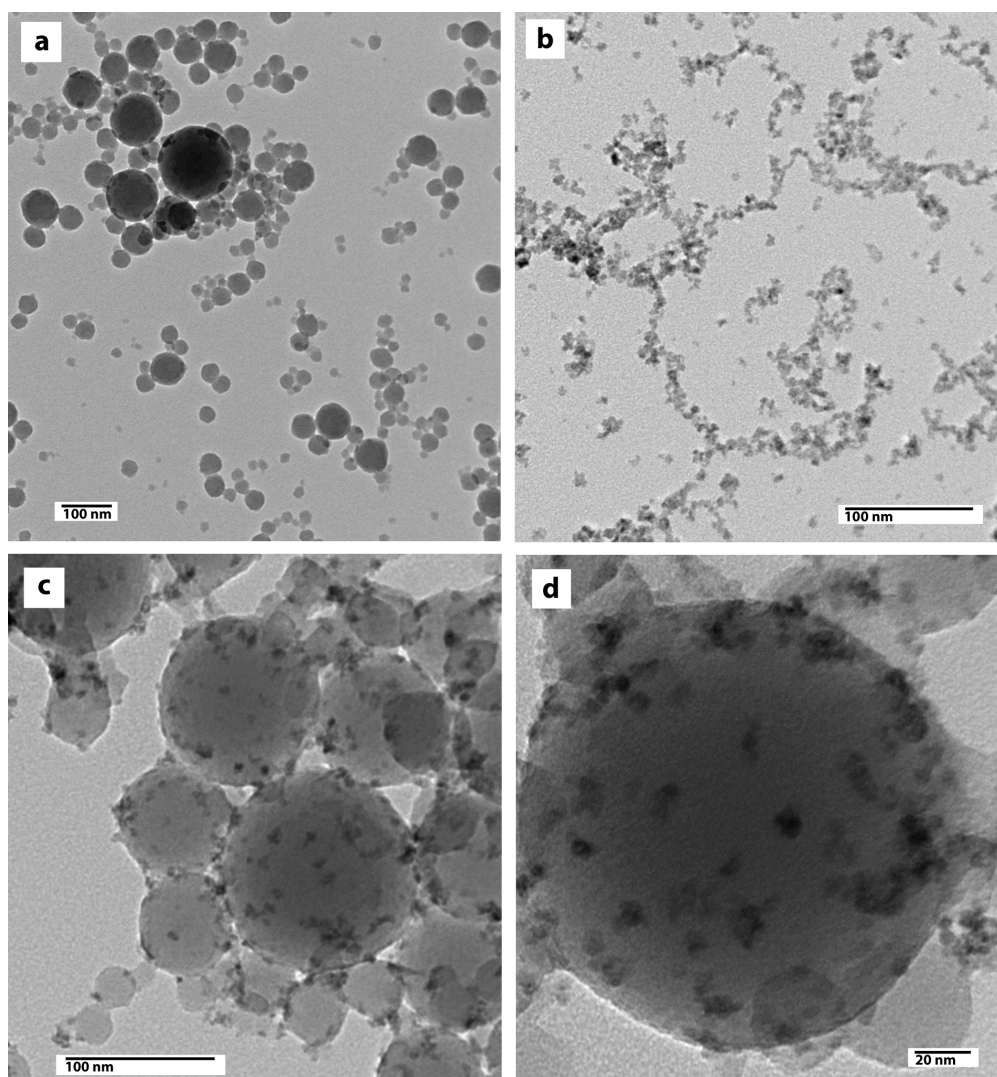


Figure 17 TEM images: (a) silica EB6080 particles—100k \times ; (b) ceria particles—250k \times ; (c) mixture of ceria with silica particles at weight ratio of 0.1—250k \times ; (d) mixture at weight ratio of 0.1—500k.

The images of silica EB6080 (19a) and ceria (19b) suggest aggregation of dry particles on the TEM grids, despite the fact that there was a strong repulsion force between silica particles in suspension, which held true for silica particles. This was probably due to the surface tension driving particles

together as the water evaporated from the grids. This aggregation was especially apparent in ceria particles as seen in Figure 17b where a chain network of ceria particles was formed. This is because that ceria has much smaller size than silica EB6080, and thus better mobility under similar forces. The estimation of particle sizes of silica and ceria from Figure 17a and Figure 17b was roughly close to the particle size measurements shown in Table 2.

Figure 17c provides solid evidences for the hypothesis that ceria particles are attached to silica particles at pH 4 due to their opposite surface charges. A very good and well-dispersed coverage of ceria particles on the silica particle surfaces indicated that the attachments were formed before the water evaporated from the grids and most such attachments were unaffected by the surface tension during water evaporation. Had not the ceria particles attached to silica particles in solution media, well-dispersed attachments would have disappeared and a chain of ceria particles would have been seen in Figure 17c. In our study, a well-dispersed coverage of silica by ceria particles was obtained by simply mixing commercially available slurries and adjusting its pH. No further treatment such as hydrothermal reactions were conducted after mixing. Such coverage may be beneficial in oxide Chemical Mechanical Polishing. Figure 17d is an image of higher magnification of mixed particles dried from solutions at pH 4.

3.3.2 TEM of Ceria/Silica Made at pH 10

At pH 10, ceria and silica particles are both negatively charged and therefore repel each other in the solution. When the mixed abrasive solution is air dried at pH 10, the ceria and silica particles will get closer and closer despite the electrostatic repulsion, due to the surface tension of water. When all the water is evaporated, the ceria particles finally come in contact with the silica particles. However, such attachment of ceria particles to silica particles should be different from the attachment seen in Figure 17c and 17d. Since ceria particles are not attached to silica particles during evaporation at pH 10, the ceria particles will aggregate on their own just as shown in Figure 17b. (Ceria particles dried from pH 10 solution under TEM are believed to look similar as

those dried from pH 4.) Therefore, TEM images of such mixed particles evaporated from solution of pH 10 should contain a network of ceria particles aggregating together, attaching to silica particles, but not a well-dispersed coating of ceria formed on silica particles as seen in Figure 17c and 17d. Figure 18 is an image of this situation.

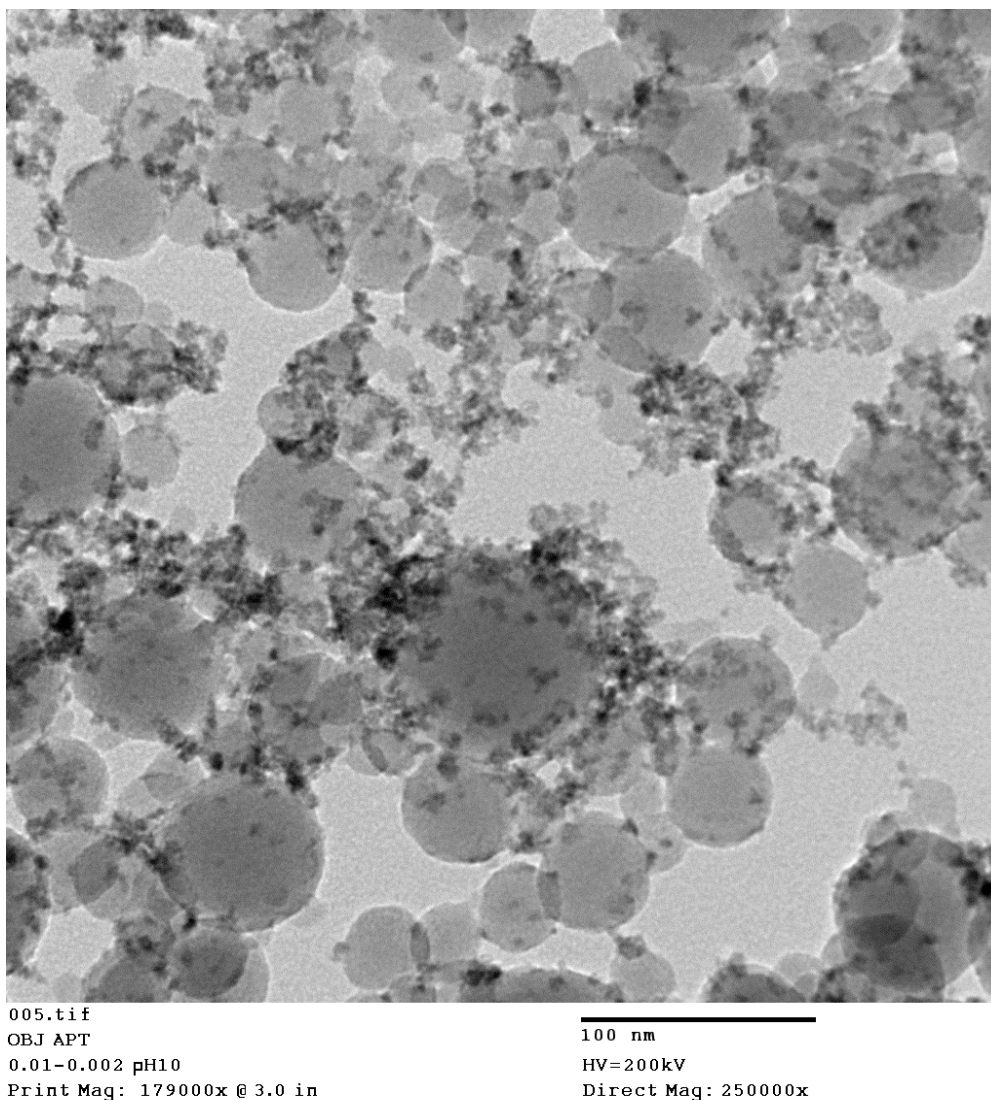


Figure 18 TEM image of ceria with silica particles (dried from solution at pH 10)

A clear network and aggregation of ceria particles seen in Figure 18 attests to the previous discussions. It needs to be pointed out that the sample (ceria-to-silica weight ratio 0.2) used for obtaining Figure 18 had twice the ceria-to-silica weight ratio as the sample (ceria-to-silica weight ratio 0.1) used for obtaining Figure 17c had, in addition to that there was a difference in solution

pH values. However, samples with the same weight ratio of 0.1 as used in Figure 17c had similar ceria network formation at pH 10, similar as what is shown in Figure 18.

In Figure 18, no well-dispersed coverage of ceria particles on silica particle surfaces is seen. However, there are a few distinct individual ceria particles seen on silica surface. This is believed to be very normal as there is chance of some individual ceria particles not aggregating to their own species, just as the few distinct ceria particles seen in Figure 17b. Another possible reason for this is that ceria and silica formed a bond of Ce-O-Si at a high pH of 10 solution, as illustrated in equation (3). Such bonding could be formed during the collision of ceria particle to silica particle due to Brownian motions. Once the bond was formed, the ceria particle was bound to the silica surface despite the surface tension of water during the drying process.

In summary, this section has demonstrated the capability and usefulness of TEM. The results of TEM have provided solid support toward our hypothesis of ceria attachment to silica when they are oppositely charged, based on our mathematical model of equation (15).

3.4 CMP EFFICIENCY OF MIXED ABRASIVE SLURRIES

3.4.1 Effect of Ceria Addition to Silica on CMP of Oxide

Figure 19 shows the PECVD silicon dioxide polishing rates using silica EB6080 (5 wt%) slurries and mixed slurries containing 5 wt% silica EB6080 and 1 wt% ceria at pH 4 under various down pressures. The two lines are the linear regressions of the two data series. All silica particles used in polishing experiments were silica EB6080. Unless indicated otherwise, the pH of the slurries used was adjusted to 4. Silica weight percentage was 5 wt%.

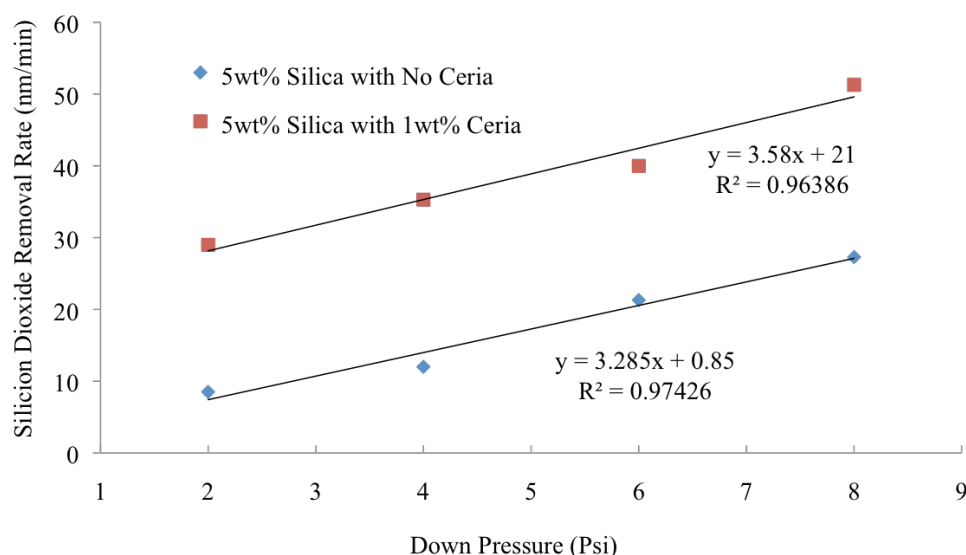


Figure 19 Oxide Removal Rates using silica slurries and mixed slurries at pH 4

In our initial polishing experiments using 1 wt% ceria slurries at pH 4, the polishing rate was about 2 nm/min at a down pressure of 4 psi. This is believed to be caused by the very small size of ceria particles. Meanwhile, slurries with 5 wt% silica particles only polished oxide at a rate of about 12 nm/min at pH 4 and 4 psi down pressure. By combining the two particles within one slurry, mixed abrasive slurries containing 5 wt% silica and 1 wt% ceria at pH 4 had an oxide polishing rate of approximately 35.3 nm/min, which is about 3 times the polishing rate of silica and 18 times the polishing rate of ceria under same conditions. Such synergistic effect was also seen in

polishing experiments carried out at lower and higher down pressures as shown in Figure 19.

Several reasons could be responsible for the increase in oxide polishing rates due to addition of ceria particles. Firstly, the synergistic effect was largely due to the combination of mechanical forces from the silica particles under pressure and the chemical tooth effect of ceria particles on oxide film surfaces during polishing. The low polishing rates using ceria alone, compared to those reported in other studies (Y.-H. Kim et al., 2008; P. R. D. Veera et al., 2009), were due to the fact that the ceria particles were very small in size as mentioned previously, which could not effectively transfer the mechanical shearing forces from the polishing pad to the oxide film surface. The presence of much larger silica particles within the mixed slurries solved this problem, which also probably increased the contact area between ceria particles and oxide film surface being polished. From the other point of view, the hydrolysis of oxide film surface was less efficient at pH 4 than high pH values or basic regions, which may be the reason for low oxide polishing rate using slurries containing only silica particles. The chemical tooth effect from addition of ceria particles was a big supplement in this case. Therefore, by combining the advantages of the two kinds of particles, mixed abrasive slurries worked better than single-component slurries. Secondly, the ceria-coated silica particles within in this slurry, which had a ceria-to-silica weight ratio of 0.2, had a zeta potential of about +39 mV according to the measurement results shown in Figure 10, and a little lower than +30 mV according to Figure 13. Meanwhile, the silicon dioxide film deposited on silicon substrate had a negative zeta potential of about -32 mV. Therefore, the mixed abrasives were likely attached to silicon dioxide thin film surface. The ceria particles acted as a bridge, connecting the silica abrasives and silicon dioxide film surface. Such bridging effect of ceria particles increased the efficiency of stress transferring from silica particles to silicon dioxide film surface. Without the presence of ceria particles as a bridge, the silica particles were negatively charged and repelled from the oxide film surface. Therefore, the bridging effect of ceria particles was essential to increase the amount of silica particles attached to oxide film surface, which was favored for high polishing rates.

As discovered previously, mixed abrasive slurries with weight ratio of 0.05-0.15 had very poor stability. This can be an indicator of high material removal rates since the particles within the slurries aggregated and can be in contact with surface to be polished easily under polishing pressure. Figure 20 is a comparison of oxide polishing rates between silica slurries, ceria slurries, and mixed slurries with weight ratios from 0.02 to 0.3, at pH 4.



Figure 20 Oxide polishing rates using silica slurry (5 wt%), ceria slurries (0.1 wt%, 0.5 wt% and 1.5 wt% from left to right) and mixed slurries of silica and ceria at pH 4

NOTE: Within each group of columns, silica slurry is on the left, ceria slurry is in the middle and mixed slurry is on the right side

Similarly, synergistic effect is also seen in Figure 20, or oxide polishing with low weight ratio mixed slurries at pH 4. When ceria and silica slurries were added to each other, the resulted mixed abrasive slurries showed a significant increase in oxide polishing rates, especially at ceria-to-silica weight ratio of 0.1 as shown in Figure 20. The three groups of polishing results correlated well with the previously discussed zeta potential measurements, settling tests and TEM images. At the weight ratio of 0.1, mixed abrasive slurries with 5 wt% silica particles and 0.5 wt% ceria particles had an oxide polishing rate 284.6 nm/min, which is more than 20 times the oxide polishing rate of silica slurry. Accordingly, at the same weight ratio, the slurry had poor colloidal stability as suggested in Figure 15 due to the attachments of ceria particles on

silica particle surfaces (Figure 17), which resulted in the change of the zeta potentials of ceria-coated silica particles within the slurry. This enhancement in oxide polishing rates was more significant than the previously mentioned studies using ceria and silica nanoparticles (Z. Lu et al., 2003; S.-H. Lee et al., 2002).

3.4.2 Effect of Ceria Addition to Silica on CMP of Nitride

Using the same slurries at same conditions, nitride polishing was conducted. The following Figure 21 plots the nitride removal rates as a function of down pressure applied from the wafer carrier. The two lines are the linear regressions of the two data series.

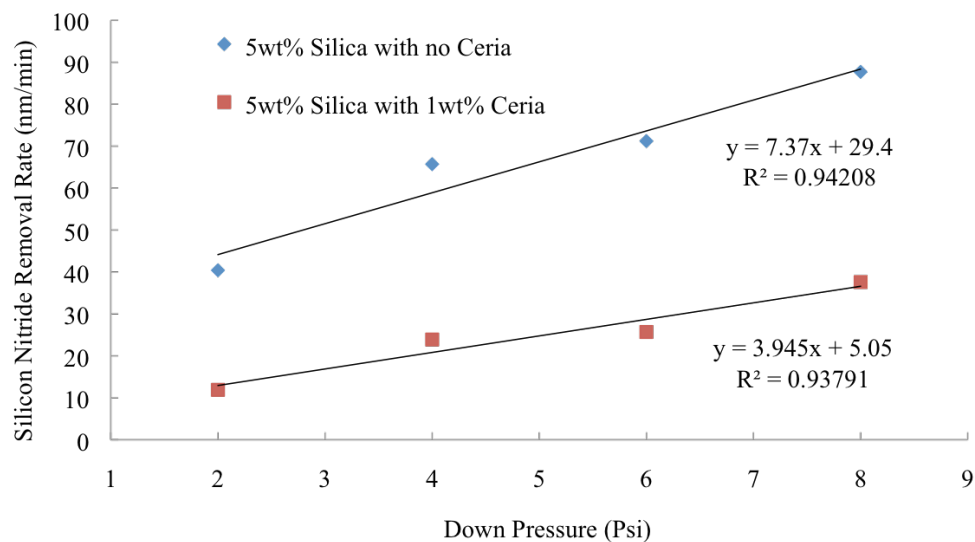


Figure 21 Nitride Removal Rates using silica slurries and mixed slurries at pH 4

Slurries with only silica particles polished nitride at fairly high rates. This was probably due to the fact that negatively charged silica particles were attracted to positive nitride film surfaces at pH 4. The mechanical factor in this case was dominating the polishing rates.

It is clear that adding certain amount of ceria to silica slurries suppressed the nitride polishing by 3 to 4 times in this weight ratio, according to Figure 21. The chemical process of nitride polishing contains two steps as shown in equation (4) and equation (2): converting Si-N-Si bond to oxide, and

hydrolysis of oxide. The first step is usually more difficult than the second step. Especially, the ceria-coated silica particles had positive zeta potentials, and were repelled from the nitride surfaces at pH 4 because nitride had about +25 mV at this pH. Therefore, a decrease in nitride removal rates was observed with this mixed slurry at all tested down pressures. This decrease in nitride polishing rate is favored by STI CMP since it desires a good oxide to nitride selectivity.

However, it is very necessary to point out that, such depression in nitride polishing is believed to be typically seen in polishing with slurries at ceria-to-silica weight ratios higher than 0.2. As the ceria-to-silica weight ratio is lowered from 0.2, the ceria-coated silica has decreasing zeta potentials, reducing the repulsion strength between ceria-coated silica particles and nitride film surface. This repulsion will disappear and turn into attraction when ceria-coated silica particles are negatively charged at low enough weight ratios. In addition, the mixed slurries will become unstable when the weight ratio is decreased from 0.2 to 0.05. This increase in instability may adversely increase the nitride polishing rates (as well as oxide polishing rates, but favorably). Using mixed slurries with ceria-to-silica weight ratio of 0.1 and 0.05, the nitride was polished at rates of 147.1 nm/min and 113.5 nm/min, respectively at pH 4 and 4 psi. These rates are much higher than using slurries with silica alone under same conditions. This increase was due to the instability of the mixed slurry, while slurries with silica alone had good stability at pH 4. The instability increased the chance of more ceria-coated silica particles contacting the nitride surfaces under polishing pressure, similar to the situations of oxide polishing. The exact results of nitride polishing using low weight ratio slurries are not shown here. Figure 22 attests the nitride polishing suppression effect of slurries with higher (than 0.2) ceria-to-silica weight ratios, which agrees with the discussions following Figure 21.

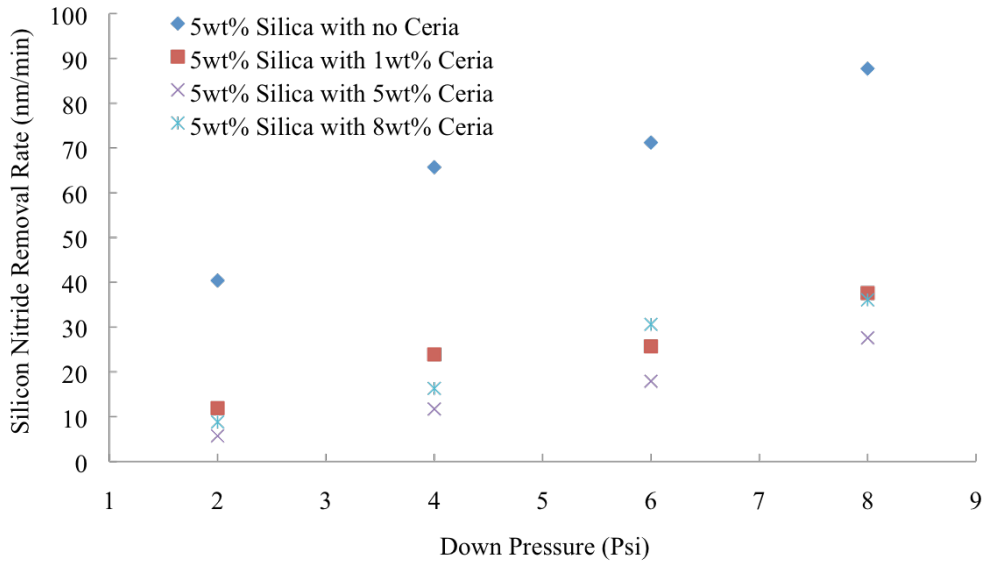


Figure 22 Nitride Removal Rate with Slurries of higher weight ratios at pH 4

3.4.3 Comparison of CMP Efficiency at Different pHs

A comparison of oxide and nitride polishing rates using mixed abrasive slurries with weight ratio of 0.1 at different pH was carried out. The process parameters for the experiments were the same as described in Table 1. The only difference between the two kinds of slurries used was the pH.

It is demonstrated in Figure 23 that when the pH of such mixed abrasive slurry was increased to 10, the oxide polishing rate dropped to 45.3 nm/min from the original 284.6 nm/min at pH 4, despite that the hydrolysis reaction of oxide film surface was stronger at pH 10. Settling test of this slurry at pH 10 proved that it had much better colloidal stability, which was confirmed by the zeta potential results in Figure 13. This increase in stability, caused by the electrostatic repulsion between ceria and silica particles at pH 10, was also the reason for the decrease in nitride removal rate from 147.1 nm/min to 52.1 nm/min when pH was changed from 4 to 10. Therefore, it is suggested that the synergistic effect of ceria and silica particles in this study work best when a well-dispersed coating of ceria particles is formed on silica particle surfaces, and when the slurry reaches its minimum colloidal stability. However, more studies need to be done in order to reduce the nitride removal rates to increase polishing selectivity for STI CMP.

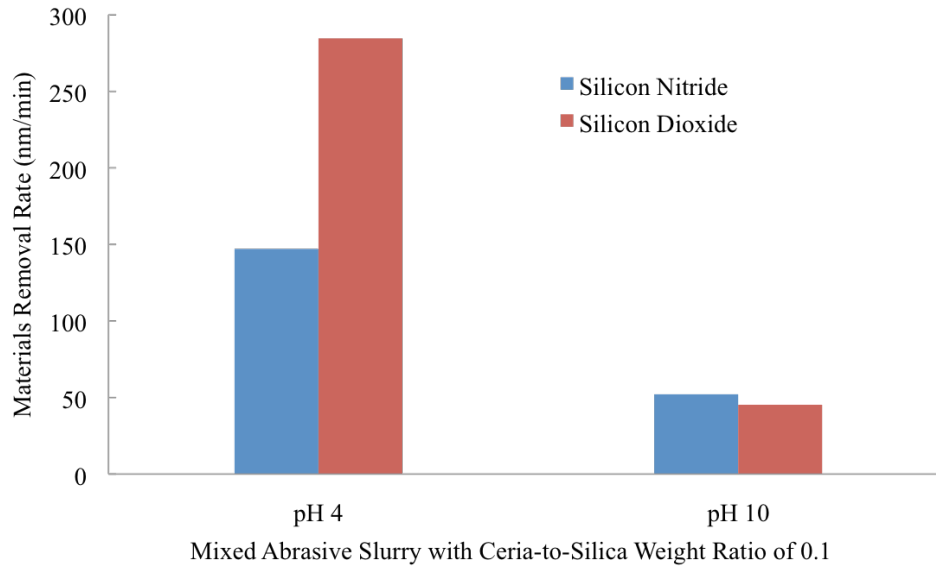


Figure 23 Comparison of Materials Removal Rates at pH 4 and pH 10

3.4.4 Schematic Model of Oxide CMP at pH 4

Based on section 3.4.1 and 3.4.2, the synergistic effect of mixed abrasive slurries for oxide polishing at pH 4 is outlined in Figure 24.

At very low ceria-to-silica weight ratios, the ceria-coated silica particles are negatively charged and are repelled from the oxide surface, which also has negative charge at pH 4. The ceria-coated silica particles also repel each other so the slurry is fairly stable. This case is illustrated in Figure 24(a), where some particles are attached to oxide surface due to the bridging effect of ceria, and particles are separated from each other at a good distance. Therefore in the case of Figure 24(a), the synergistic effect may not be apparent because of the small amount of ceria particles within the slurry and the repulsion forces between particles and oxide surface.

In the case of Figure 24(b), more ceria particles are attached to silica particle surfaces and the amount of net surface charge is significantly reduced to near-zero. Therefore, the slurry is unstable and aggregation is seen. Under the polishing pressure, these aggregated particles can be easily pushed upon the oxide surface, and generate very high oxide polishing rates, with sufficient

amount of ceria particles reacting with the oxide surface. At this point, the synergistic effect is most obvious.

In the case shown in Figure 24(c), ceria-coated silica particles have high positive negative charge; therefore, good attachment of such particles on oxide surface is seen. But since the positive charged particles repel each other, fewer particles are able to get close and attach to oxide surface compared to the particles in case (b). Therefore the synergistic effect in case (c) is not as strong as case (b). But compared to the case (a), since particles in case (c) are oppositely charged to the oxide surface, more mixed particles are attached to oxide surface. Therefore, the synergistic effect should be more obvious in case (c) than case (a) (chemical tooth effect is also stronger in case (c)).

To summarize, at pH 4 (silica and ceria particles and oppositely charged), mixed abrasive slurries with weight ratios inside the transition range have the most significant synergistic effect in oxide polishing (increase of oxide removal rates) because the instability of the slurries allows many aggregated particles contacting the oxide film surface under the polishing pressure. Mixed abrasive slurries with weigh ratios below the transition range have the least significant increase of oxide removal rates over slurries containing silica alone because the negatively charged mixed particles (ceria-coated) are repelled from the oxide film surface, and that chemical tooth effect is limited due to low levels of ceria amount. The slurries with weigh ratios higher than the transition range falls between these two cases.

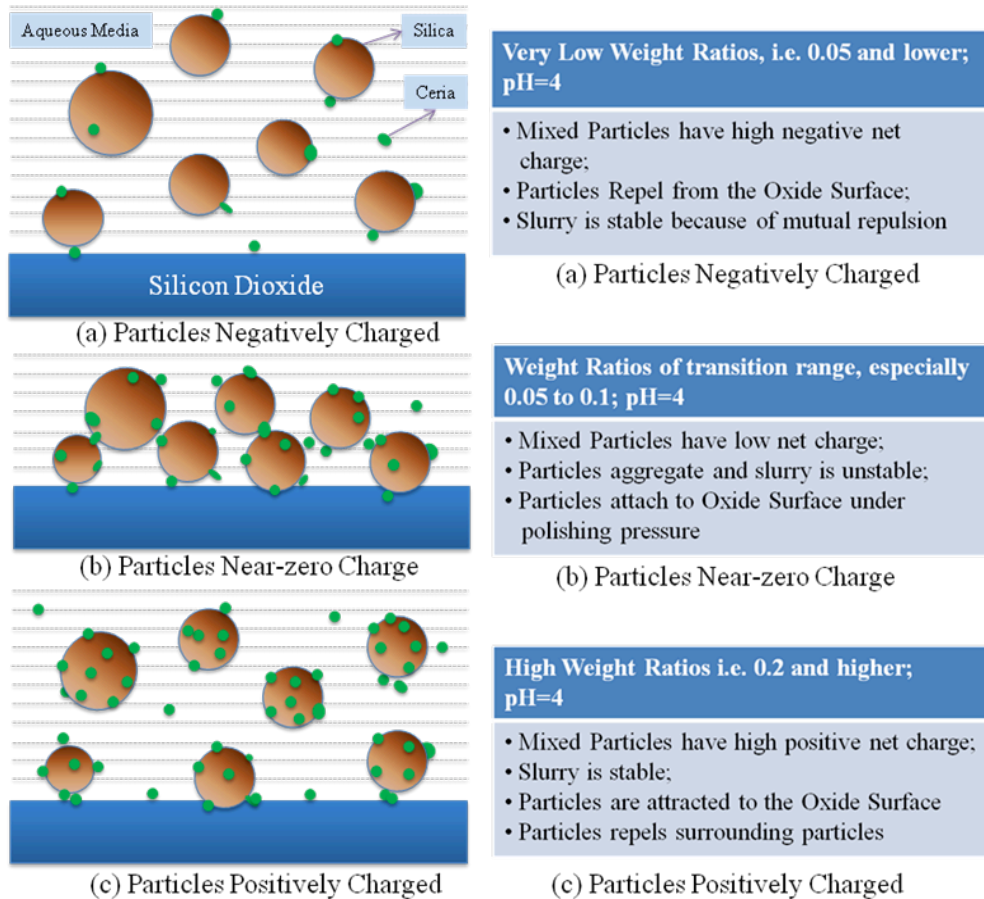


Figure 24 Oxide Polishing Model at pH 4 for various weight ratios: (a) very low weight ratio i.e. 0.02, particles negatively charged; (b) weight ratios of transition range, particles slightly charged or near-zero charge; (c) higher weight ratios, i.e. 0.2 and above, particles positively charged

If we compare this analysis with the polishing results of mixed slurries shown in Figure 20, good agreement is found. Mixed abrasive slurry with a weight ratio of 0.02 had oxide removal rate of 46.6 nm/min (corresponding to the case of Figure 24(a)), 285 nm/min for slurry with weight ratio of 0.1 (corresponding to the case of Figure 24(b)), and 63.6 nm/min for weight ratio of 0.3 (corresponding to the case of Figure 24(c)). Note that the notional transition range for mixed slurries of silica EB6080 and ceria at pH 4 is approximately 0.05 to 0.1 as discussed in Figure 10 and Figure 15.

Similar analysis can also be done to nitride polishing at pH 4 but is not presented in this thesis.

CHAPTER 4 CONCLUSIONS & FUTURE WORK RECOMMENDATIONS

4.1 CONCLUSIONS

The colloidal stability of mixed abrasive slurries (MAS) containing silica and ceria nanoparticles has been evaluated. MAS made by mixing commercially available silica slurries and ceria slurries exhibited a transition in slurry stability that occurs in the weight ratio of ceria over silica between 0.05~0.3 for all tested silica slurries. This transition was explained by the hypothesis of modification of particle surface charge through the attachment of ceria nanoparticles to silica nanoparticles when they were oppositely charged, which was confirmed by zeta potential measurements and transmission electron micrographs. The weight ratio between ceria and silica particles of zero net surface charge was found to be dependent on the pH of MAS (ζ -potential of particles) and average particle sizes (overall particle surface area). The MAS outside of the transition range regained good stability. The CMP performances of oxide thin films using such mixed abrasive slurries were presented, and a synergistic effect between the two kinds of particles was observed and explained. By adding the right (usually little) amount of ceria particles to silica slurries, the oxide polishing rate was increased by 20 times from 14 nm/min using silica to 284 nm/min using mixed abrasive slurries at pH 4.

4.2 FUTURE WORK RECOMMENDATIONS

Since the initial intension for a mixed abrasive slurry study was for the applications in Shallow Trench Isolation Chemical Mechanical Polishing, future work should include the STI CMP performance of such mixed abrasive slurries. Studies on the effect of chemical additives, surfactants and pH to the slurries and the slurries' STI CMP performances can also be included in future work in order to develop slurries with good oxide-to-nitride selectivity and surface finish. Mixed abrasive slurries using other kinds of particles can be also studied for their STI CMP performances.

Further characterizations of the mixed abrasive slurries can be carried out. For example, the mixed abrasive slurries containing the two kinds of particles were observed to have different viscosities at different ceria-to-silica weight ratios. It would be informative to have the characteristics of such slurries in viscosity and other rheology parameters.

The study of mechanisms of oxide and nitride polishing using the mixed slurries or single-component slurries is also a good area of future work. Such study can be conducted through friction measurements using a system that can measure the carrier motor current. In addition, Surface Force Apparatus may be a good technique to study the frictions between particles and surfaces under various conditions. These studies should be able to shed light on the polishing mechanisms.

References

A. Einstein, Investigations on the theory of the Brownian movement, Dover Publications, New York, 1956.

A. Bryant, W. Haensch, T. Mii, Characteristics of CMOS device isolation for the ULSI Age, IEDM Technical Digest, (1994) 671-674.

A. S. Dukhin, P. J. Goetz, in: D. Mobius, R. Miller (Eds.), Ultrasound for Characterizing Colloids: Particle sizing, Zeta potential, Rheology, Elsevier Science B. V., Amsterdam, 2002.

A. Jindal, S. Hegde, S. V. Babu, Journal of Electrochemical Society 150 (2003) G314-G318.

A. Philipossian, S. Olsen, Materials Research Society Symposium Proceedings 767 (2003) F2.8.1-F2.8.7.

A. Philipossian, E. Mitchell, Journal of Electrochemical Society 151 (6) (2004) G402-G407.

B. D. Tang, Dissertation PhD: Characterization and Modeling of Polysilicon MEMS Chemical-Mechanical Polishing, Massachusetts Institute of Technology, 2004. Available online:

<http://dspace.mit.edu/bitstream/handle/1721.1/17983/57189433.pdf>

D. Atwood, Soft X-rays and Extreme Ultraviolet Radiation, Principles and Application, University of Cambridge Press, 1999, Chapter 10.

F. B. Kaufman et al., Chemical-Mechanical Polishing for fabricating W metal features as chip interconnects, Journal of Electrochemical Society 138 (11) 3460-3465.

H.-C.Kim, H.M. Lim, D.-S. Kim, S.-H. Lee, Transactions on Electrical and

Electronic Materials 7 (4) (2006) 167-172.

H. J. Levinson, Principles of Lithography, 3rd ed., SPIE Press, Bellingham, 2010, pp. 7-47. Available from University of Alberta Library Internet.

H. J. Levinson, Principles of Lithography, 3rd ed., SPIE Press, Bellingham, 2010, Chapter 12 pp. 425-458. Available from University of Alberta Library Internet.

J. J. Sniegowski, Chemical Mechanical Polishing: enhancing the manufacturability of MEMS, Micromachining and Microfabrication Process Technology II Proceedings 2879 (1996) 104-115.

J. M. Steigerwarld, S. P. Murarka, R. J. Gutmann, Chemical Mechanical Planarization of Microelectronic Materials, Wiley, New York, 1996

J. Liu, Z. Zhou, Z. Xu, J. Masliyah, Journal of Colloid and Interface Science 252 (2002) 409-418.

J. Kim, U. Paik, Y.-G. Jung, T. Katoh, J.-G. Park, Japanese Journal of Applied Physics 41 (2002) 4509–4512.

J. T. Abiade, Dissertation PhD: Characterization of the Chemical Effects of Ceria Slurries for Dielectric Chemical Mechanical Polishing, University of Florida, Gainesville, 2004.

K. S. Birdi, Surface and Colloid Chemistry: Principles and Applications, CRC Press, Boca Raton, 2010, pp. 141-159.

K. Hosono (Ed.), Photomask and Next-Generation Lithography Mask Technology XVII, Proceedings of SPIE, 7748 (2010). Available online: <http://www.gbv.de/dms/tib-ub-hannover/636071758.pdf>

L. M. Cook, Journal of Non-Crystalline Solids 120 (1990) 152-171.

M. Fayolle, E. Sicurani, Y. Morand, W CMP process integration: consumables evaluation—electrical results and end point detection. *Journal of Microelectronic Engineering* 37-38 (1997).

M. R. Oliver, Integration Issues with Cu CMP, CMP Users Group, Press release Rodel Inc (2003).

M. Krishnan, J. W. Nalaskowski, L. M. Cook, *Chemical Reviews* 110 (2010) 178–204.

M. Altissimo, E-beam lithography for micro-/nanofabrication, *Biomicrofluidics* © American Institute of Physics 4 (2010).

N. Nishiguchi, T. Uen, M. Kawaguchi, *Journal of Dispersion Science and Technology* 31 (2) (2010) 149–154.

P. W. Carter, T. P. Johns, *Electrochemical and Solid-State Letters* 8 (8) (2005) G218-G221.

P. R. D. Veera, S. Peddeti, S. V. Babu, *Journal of Electrochemical Society* 156 (12) (2009) H936-H943.

R. Doering, Y. Nishi (Eds.), *Handbook of Semiconductor Manufacturing Technology*, Marcel Dekker, New York, 2000.

R. Manivannan, S. Ramanathan, *Journal of Microelectronic Engineering* 85 (2008) 1748–1753.

S. P. Murarka, I. V. Verner, R. J. Gutmann, *Copper—Fundamental Mechanism for Microelectric Applications*, Wiley, 2000.

S.-H. Lee, Z. Lu, S. V. Babu, E. Matijevic, *Journal of Materials Research* 17 (10) (2002) 2744-2749.

S. W. Jones, A simulation study of the cost and economics of 450 mm wafers, 2005.

S. Kim, J.-H. So, D.-J. Lee, S.-M. Yang, Journal of Colloid and Interface Science 319 (2008) 48-52.

S. Li, G. Gaudet, F. Sun, A. Naman, Journal of Electrochemical Society 157 (11) (2010) H1061-H1066.

T. Matsuzaka, Y. Soda, Electron Beam Lithography System for Nanometer Fabrication, Hitachi Review 48 (6) (1999) 340-343.

U. Paik, J.-G. Park, Nanoparticle Engineering for Chemical-Mechanical Planarization: Fabrication of Next-Generation Nanodevices, CRC Press, Boca Raton, 2009, pp. 3-8.

U. Paik, J.-G. Park, Nanoparticle Engineering for Chemical-Mechanical Planarization: Fabrication of Next-Generation Nanodevices, CRC, Boca Raton, 2009, pp. 9-33.

V. Baksh (Ed.), EUV Sources for Lithography, SPIE, Bellingham, 2005.

W.G. America, S.V. Babu, Electrochemical and Solid-State Letters 7 (12) (2004) G327-G330.

W. Choi, R. K. Singh, Japanese Journal of Applied Physics 44 (12) (2005) pp. 8383–8390.

Y.-J. Seo, W-S Lee, Effect of oxidants for exact selectivity control of W and Ti CMP process, Journal of Microelectronic Engineering 77 (2005) 132-138.

Y. Li (Ed.), Microelectronic Applications of Chemical Mechanical Planarization, Wiley Interscience, New Jersey, 2007.

Y.-H. Kim, S.-M. Lee, K.-J. Lee, U. Paik, *Journal of Materials Research* 23 (1) (2008) 49-54

Z. Lu, S.-H. Lee, V. R.K. Gorantla, S. V. Babu, E. Matijevic, *Journal of Materials Research* 18 (10) (2003) 2323-2330.